

Spring 2020

Microfluidic Liquid Biopsy for Cancer Prognosis

Brendan Heap

Anthony Ramirez Guerrero

Sam Nichols

Follow this and additional works at: https://scholarcommons.scu.edu/bioe_senior



Part of the [Biomedical Engineering and Bioengineering Commons](#)

Recommended Citation

Heap, Brendan; Guerrero, Anthony Ramirez; and Nichols, Sam, "Microfluidic Liquid Biopsy for Cancer Prognosis" (2020). *Bioengineering Senior Theses*. 95.

https://scholarcommons.scu.edu/bioe_senior/95

This Thesis is brought to you for free and open access by the Engineering Senior Theses at Scholar Commons. It has been accepted for inclusion in Bioengineering Senior Theses by an authorized administrator of Scholar Commons. For more information, please contact rscroggin@scu.edu.

SANTA CLARA UNIVERSITY

Department of Bioengineering

I HEREBY RECOMMEND THAT THE THESIS PREPARED
UNDER MY SUPERVISION BY

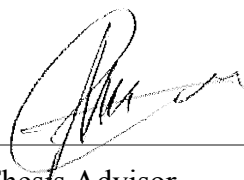
Brendan Heap, Anthony Ramirez Guerrero, Sam Nichols

ENTITLED

**Microfluidic Liquid Biopsy for
Cancer Prognosis**

BE ACCEPTED IN PARTIAL FULFILLMENT OF THE
REQUIREMENTS FOR THE DEGREES OF

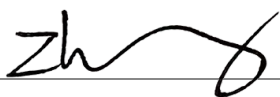
**BACHELOR OF SCIENCE
IN
BIOENGINEERING**



Thesis Advisor

June 11, 2020

Date



Department Chair

June 11, 2020

Date

Microfluidic Liquid Biopsy for Cancer Prognosis

by

Brendan Heap
Anthony Ramirez Guerrero
Sam Nichols

SENIOR DESIGN PROJECT REPORT

Submitted to the Department of Bioengineering

of

SANTA CLARA UNIVERSITY

in partial fulfillment of the requirements for the degree of Bachelor
of Science in Bioengineering

Santa Clara, California

Spring 2020

Abstract

Leukemia is a deadly and common cancer, especially in children and adolescents. The misdiagnosis and unexpected complications during the treatment are some factors that increase the mortality rate of leukemia. The goal of our project was to create a device that would quickly and accurately assess these complications. While there are existing tests that can perform a single test for either metastasis or sepsis, there are none that can test for both simultaneously and rapidly. We propose to modify and combine some of these existing microfluidic designs as well as create a new component to perform a combinatorial assessment. While we were unable to verify the results, we have designed a device that will potentially meet our goals of testing for sepsis, severe sepsis, solid-body metastasis risk, major solid-body metastasis risk, lymphoma metastasis risk, and progression of the primary blood-based cancer (leukemia/lymphoma), from 7.5 mL of blood in just under 2 hours. We believe that this device has the potential to contribute to the medical field due to its speed and efficiency, especially in a pediatric demographic.

Acknowledgements

We would like to thank the head of the Bioengineering Department, Dr. Zhiwen Zhang, for his assistance in starting us down the path that ultimately led to this project.

We would like to thank our project advisor, Dr. Emre Araci, for getting our team up to speed with our project after several complications that were out of our control forced us to switch project advisors and start a new project. We thank him for believing in us, for his honest and thorough feedback, and his guidance and support throughout this project.

We would also like to thank Dr. Prashanth Asuri for his honest and thorough feedback on our capstone presentations, which helped us organize our thesis.

We would like to thank our friends and families for their tireless love and support through this process. Through the long nights and stressful days, you were there for us. We could not have done this without you.

Finally, we would like to thank Santa Clara School of Engineering for funding and supporting our project, as well as providing us with an unforgettable educational experience that has allowed us to grow in a multitude of ways.

Table of Contents

Abstract	2
Acknowledgements	3
Chapter 1: Introduction	8-12
Chapter 2: Project Overview	12-14
Chapter 3: Background and Significance	
3.1 Background and Motivation of Subject Matter	14-16
3.2 Microfluidics	16-17
3.3 Labyrinth Microfluidic Device for CTC Filtration	17-19
3.4 Sepsis and Mechanism of Propagation	20
3.5 Molecular Beacons for Enumeration of mRNA	21-22
Chapter 4: Subsystems Overview	
4.1 Pillar Chip	22-24
4.2 Labyrinth Chip	24-27
4.3 CD64 mRNA Expression Chip	28-30
Chapter 5: System Integration	30-33
Chapter 6: Results	
6.1 Hypothetical Pillar Data	33-34
6.2 Hypothetical Labyrinth Data	34-37
6.3 Hypothetical Sepsis Assessment Data	37-38
Chapter 7: Engineering Standards	
7.1 Manufacturability	38-39
7.2 Environmental/Sustainability	39
7.3 Economic/Social/Political	39-40
7.4 Ethical/Health and Safety	40
Chapter 8: Summary and Conclusion	40-42
Appendix	
A.1 Additional Information: Electrode Cell Counter	43
A.2 Additional Information: CTCC Separator Stage 2	43-44
A.3 Requirement List	45
A.4 Sketches/Alternate Designs	45-50
A.5 Decision Rationale	50-51
A.6 Calculations	52-57
A.7 Academic Timeline for Microfluidic Liquid Biopsy for Cancer Prognosis	58
A.8 Literature Review	58-80
Bibliography	80-86

List of Figures

- Figure 1.1:** Cartoon sketch of the localization of LM tumor in the brain and spine. 10
- Figure 3.1:** Cartoon sketch depicting CTC and CTCC mechanisms of movement in a blood vessel from a primary tumor. 15
- Figure 3.2:** Visual representation of the Dean coupled inertial focusing profiles of particles in a curved low aspect ratio microchannel. 18
- Figure 3.3:** SEM image of sharp corners in Labyrinth that enhance Dean forces. 19
- Figure 3.4:** Sketch of the binding mechanism for molecular beacons, with the unbound beacon shown on the left and the bound beacons shown on the right. 21
- Figure 3.5:** Cartoon sketch of a triple fluorophore/quencher molecular beacon shown on the left, with a graph of the relative fluorescence of different molecular beacon designs on the right. 22
- Figure 4.1:** Cartoon sketch diagramming the mechanism of large cluster separation through deterministic lateral displacement. 23
- Figure 4.2:** Cluster separation microfluidic chip AutoCAD design with blood and buffer entering through the top of the chip and separated clusters exiting on the bottom right. 24
- Figure 4.3:** Long loops and sharp corners in Labyrinth result in clean and separated focusing of CTCs and small WBCs. 24
- Figure 4.4:** Labyrinth chip AutoCAD sketch with extra valve to pump buffer into the inlet. Color added to illustrate layer differentiation based on component height. 25
- Figure 4.5:** Inertial lift force equation showing that the magnitude of the inertial lift force is proportional to the fourth power of particle diameter, which proves that smaller particles are harder to focus. 26
- Figure 4.6:** AutoCAD diagram of sepsis assessment in the microfluidic system with lysing and quenching pictured on the top in green, the mixing channels pictured in the middle in red, and the imaging reservoir pictured on the bottom in green. 30
- Figure 5.1:** AutoCAD design showing full system integration of the various components and control layer based chamber isolation. 30
- Figure 5.2:** Different labeled subsections with flow rates or stop times, with highlighted valve for Labyrinth flow rate increase. 32
- Figure 6.1:** Stained CTCs isolated from HCC patients. 36
- Figure 6.2:** Stained CTM isolated from HCC patients. 37
- Figure 6.3:** Graph representing the difference in expression of β -actin mRNA, labeled as control, and CD64 mRNA, labeled as inflamed NR, in inflamed and non- inflamed tissue. 37
- Figure A.1:** Electrode Cell Counter with a top-down view pictured in A, and a side view pictured in C. The Section titled B shows a picture of the electrode cell counter from the side with the current represented in white. 43
- Figure A.2:** Cartoon sketch of Stage 2 of the CTCC separator showing the DLD process. 44

Figure A.3: The original AutoCAD for the Labyrinth section based on the respective reference literature.	45
Figure A.4: The original AutoCAD for the later discarded CD64 antibody-based sepsis analyzer. Red layer symbolizes control layer. Green layer symbolizes flow layer.	46
Figure A.5: The original AutoCAD for the 2-phase CTCC separator based on the respective reference literature.	46
Figure A.6: First draft of the combined system with the 2-phase CTCC separator, Labyrinth design, and CD64 antibody-based sepsis analyzer.	47
Figure A.7: New design for sepsis analysis based on fluorescent CD64 analysis using rotary mixer and lysing/quenching maze.	47
Figure A.8: Second draft of the combined system with the 2-phase CTCC separator, Labyrinth design, and new design for sepsis analysis based on fluorescent CD64 analysis using rotary mixer and lysing/quenching maze.	48
Figure A.9: Third draft of the combined system with the first phase of the CTCC separator, Labyrinth design, and sepsis analyzer based on fluorescent CD64 analysis using rotary mixer and lysing/quenching maze. Resized valves and large imaging chamber added.	49
Figure A.10: Fourth and final draft of the combined system with the first phase of the CTCC separator, Labyrinth design, and sepsis analyzer based on fluorescent CD64 analysis using rotary mixer and lysing/quenching maze. Mixing and imaging chambers resized and pillars added to increase structural integrity. Color added to differentiate layers.	50
Figure A.11: First version of time test, calculated by design section. Time is too long, requiring design changes	52
Figure A.12: Blood component calculations, based on only WBCs needing to be analyzed for sepsis. Findings show significant time reduction for sepsis analyzer	53
Figure A.13: Second version of time test, calculated by design section and based on blood component calculations. Time is better, but still too long, requiring further design changes	54
Figure A.14: Time calculation for CTCC separator based on length. Removing Stage 2 appears to be a necessary time-saving measure eliminated by redundancy from the Labyrinth	55
Figure A.15: Third version of time test, calculated by design section and based on CTCC length calculation. Time is within 2 hours, which meets our goal	56
Figure A.16: Calculation of size of imaging chamber needed for 1-layer imaging. Size reduced to allow for 2-3 layers, reducing size needed	57

List of Abbreviations

ALL - Acute Lymphoblastic Leukemia

AJCC - American Joint Committee on
Cancer

BBC - Blood-Based Cancer
(leukemia/lymphoma)

CD64 - Cluster of Differentiation 64

CD45 - Cluster of Differentiation 45

CGM - Continuous Glucose Monitoring

CTC - Circulating Tumor Cell

CTCC - Circulating Tumor Cell Cluster

CTM - Circulating Tumor Microemboli

DAPI - 4',6-diamidino-2-phenylindole

DLD - Deterministic Lateral Displacement

FACS - Fluorescence-activated Single Cell
Sorting

HCC - Hepatocellular Carcinoma

IF - Immunofluorescence

mRNA - messenger Ribonucleic Acid

NET - Neutrophil Extracellular Traps

PDMS - Polydimethylsiloxane

qPCR - quantitative Polymerase Chain
Reaction

RBC - Red Blood Cell

SIR - Systemic Inflammatory Response

TNM - Tumor, Node, Metastasis

WBC - White Blood Cell

MB - Molecular Beacon

Chapter 1: Introduction

Cancer is the second leading cause of death globally, accounting for an estimated 9.6 million deaths in 2018¹. To put this in a simpler perspective, about 1 in 6 deaths is due to cancer¹. However, adults are not the only ones being affected by cancer. Every day, 43 children are diagnosed with cancer, with an average age of diagnosis of 6 years old². Pediatric cancer may only account for less than one percent of all cancers, but that still becomes a number equaling 11,050 children in the United States under the age of 15 being diagnosed with cancer in 2020. The American Cancer Society states that of these, “about 1,190 children under the age of 15 are expected to die from cancer in 2020”³, placing cancer as the second leading cause of death for children under the age of 14, only after accidents³. There may currently be approximately 375,000 adult survivors of child cancer⁴, but 60% of them will “suffer devastating late effects such as secondary cancers, muscular difficulties and infertility”⁴. This is why we will be focusing on a primarily pediatric demographic. When identified early, cancer is more likely to respond to effective treatment and can result in a greater probability of surviving, less morbidity, and less expensive treatment¹. While screening and imaging methods can be effective for certain cancer types, they are not the most accurate and can be prone to error. There are additional hurdles with diagnosis and treatment, both due to sepsis and the nature of leukemia/lymphoma (hereon referred to as Blood-Based Cancers, or BBCs). We believe that the solution to this issue is to develop a liquid biopsy tool in the form of a microfluidic device that is inexpensive to manufacture, widely distributable, easy to use, gives rapid results, and most importantly can detect circulating tumor cell clusters (CTCCs), circulating tumor cells (CTCs), BBC white blood cell (WBC) count, and sepsis biomarkers on a single chip from a single blood sample.

CTCs are cancerous cells that shed from the primary tumor and travel through the peripheral blood to seed metastasis and form more tumors. They are the primary source of cancer metastasis. CTCCs on the other hand are fifty-fold more metastatic than CTCs and even rarer⁵. In metastatic patients, there may be just 1-2 clusters in a 7.5 mL tube of blood⁵. One of the challenges of working with CTCCs is attempting to isolate them without breaking them into individual CTCs, as most separation methods use enough force to break these clusters apart⁵. As

such, very few devices attempt to filter CTC clusters, focusing mostly on standard CTCs. Given that metastases can be more dangerous than primary tumors, causing approximately 90% of all cancer deaths⁶, thoroughly assessing blood samples for CTCs and CTCCs is vital.

The main issue with existing devices that count CTCs or even CTCCs to determine metastasis is that they ignore BBCs. These cancers are fairly common in children, accounting for 34% of all pediatric cancers⁷, totaling approximately 4,000 children each year⁸. They also tend to not present with solid-body tumors (CTCs), but a dramatic change in WBC count. The typical WBC count can be between 4,000 - 11,000 per microliter⁹, but leukemia raises it to 100,000 - 400,000 per microliter⁹, and lymphoma can drop it to below 600 per microliter¹⁰. In fact, one of the main types of solid-body tumor that BBCs can present with is leptomeningeal metastasis (LM), a type of brain cancer metastasis that is difficult to detect, is immune to intravenous chemotherapy treatment, can be easily mistaken for stroke/behavioral disorders, and can trigger spontaneous recurrence of typically aggressive brain cancer¹¹. While it is not yet proven to be linked with LM, brain cancer also accounts for 26% of all pediatric cancers⁷. Additionally, Stage 3 cancer associated with solid-body tumors (non-BBC), can involve metastasis specifically of the lymph nodes near the site of the original tumor¹². This lymph node metastasis is commonly known as lymphoma, and can occur before other types of metastasis, which are typically associated with Stage 4 cancers¹². Pediatric Non-Hodgkin's Lymphoma (NHL) has a fairly high survival rate of between 88%-91%¹³, depending on the exact age of the patient. Even though these numbers still equate to between 120 and 160 child deaths in 2020¹³, these numbers do not account for patients with NHL as a secondary cancer via metastasis. Comparatively, pediatric leukemia has a lower survival rate of around 47%, or 1,766 child deaths in 2020¹⁴. This diagnosis can be complicated greatly by the fact that an abnormal WBC count also occurs in sepsis, causing a substantial misdiagnosis risk.

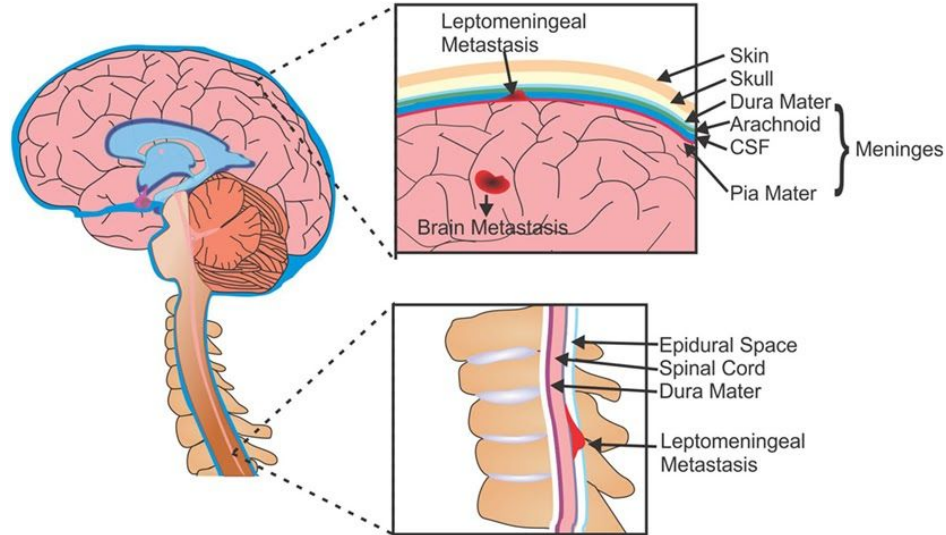


Figure 1.1: Cartoon sketch of the localization of LM tumor in the brain and spine.

Adapted from Ref. F1

Sepsis is a complication of infection, typically characterized by a “systemic inflammatory response” (SIR)¹⁵. It is life-threatening, extremely common, aggressive, and displays a wide variety of symptoms, depending on the patient. Sepsis can manifest with anything from cold/clammy skin, abdominal pain, headache, sore throat, chest pain, and many more¹⁵. Basically any symptom of most common diseases, especially infectious diseases, could be an indicator of sepsis, because it is triggered by infection. This can make it very difficult to detect by physical symptoms alone. The main symptoms of sepsis can be found within the body. Given that sepsis is a combination of SIR and an infection, we need to define what each of these are. While there are several different defining symptoms for SIR, the main one for our device is WBC count, specifically a WBC count $> 12,000/\text{microliter}$ or $< 4,000/\text{microliter}$ ¹⁵. Additionally, we can define severe sepsis (the second, more deadly phase) as sepsis additionally presenting with a platelet count $< 100,000/\text{mL}$ ¹⁵. Treatment is split, depending on the diagnosis time. Early management is implemented within 6 hours of suspected sepsis, and late management within the next 6 hours¹⁵. The ideal window for sepsis diagnosis would be within 6-7 hours of first occurrence, though sooner is preferred, because the 72-hr survival rate decreases by roughly 7.8% per hour¹⁶.

Another reason that sepsis is so important to detect early is that it can cause long-term neurological effects if sepsis interacts with chemotherapy drugs. An article by MedPage Today notes that “the neurotoxic effects of chemotherapy could alter the impact of sepsis on these patients' neurocognitive abilities”¹⁷. These effects include, but are not limited to, a 78% decrease in spatial planning, a 38% decrease in verbal fluency, a 68% decrease in inhibition, a 39% decrease in vocabulary, and a 55% decrease in visual processing speed¹⁷. Hopefully, close monitoring can lead to early detection, through which an aggressive treatment can reduce sepsis risk and reduce the chance of these harmful long-term effects.

We will be testing for all of these conditions within the same chip for several reasons. It allows for us to detect lymphoma metastasis, as well as assess leukemia progression, solid-body CTC and CTCC metastasis risk, and sepsis risk. It also allows for us to test for all of these from the same single vial of blood, rather than up to 3 individual vials. This is better for both time, and the patient's well being, as repetitive blood sampling can be hazardous for a child's health, especially during cancer treatment. We plan on having this test be available to hospitals during a child's treatment, as well as for the 7-14 day window for which they are most vulnerable to sepsis after treatment, due to a WBC chemotherapy-triggered nadir (drop)¹⁸.

With 3D printing technologies becoming more advanced and inexpensive, we hope that our microfluidic device will be able to be mass-produced at a cheap cost. The main purpose of designing this multi-step liquid biopsy tool was so that children would have access to diagnostic tools to improve their prognosis. When designing our microfluidic device, we also considered the health of our environment. We wanted to help reduce the carbon footprint by making our device as small as possible, since it cannot be reused. In addition, we wanted our device to be able to give accurate results as quickly as possible, as current liquid biopsy procedures can take up to a week to get results, for each test. This device could also be easily modifiable to target adult BBC, as well as being low-cost enough to be available to low-income communities. We believe that liquid biopsies will be the answer to improving cancer prognosis, as well as associated risks, within the child BBC demographic.

Chapter 2: Project Overview

The goal of our project is to develop a system of microfluidic tests that process a blood sample in order to assess the relative severity of BBCs and diagnose sepsis. In order to effectively do this, our project aims to accomplish several distinct and complicated diagnostic tasks. These tasks include CTC, CTCC, and WBC isolation and quantification. Each of these diagnostic tasks is completed by one of the three specific sections of the microfluidic system. The first section of the microfluidic system utilizes a pillar chip design¹⁹ to separate clusters of CTCs from the blood sample in two phases. The first section separates large CTCCs (>4 cells). The second section of the microfluidic system utilizes a labyrinth design²⁰ to separate individual CTCs, small CTCCs, and WBCs from the blood sample. The last section of the chip counts the number of WBCs which remain in the blood sample and determines the relative expression of the CD64 protein in order to diagnose and assess sepsis and BBCs within the patient.

The data collection methods for each section of the microfluidic system varies with the biological component being measured. The first two sections of the system isolate CTC clusters and individual CTCs within the sample. These cells are rare, and clusters of them even more so, so the presence of a single cell or cluster is likely indicative of a risk of metastasizing cancer and therefore the accuracy of the data is important. Both of the first two sections of the microfluidic system utilize microfabricated electrodes which generate a specific voltage spike based on the size of the cells, or group of cells, that pass through them. Therefore, this counting mechanism not only determines the count of CTCs and CTCCs but it also determines the amount of cells that are present in each cluster during the first section of the system (Appendix A.1). The third section of the microfluidic system, however, uses both microfabricated electrodes and fluorescent microscopy in order to measure different aspects of the erythrocytes and leukocytes within the blood sample. Initially, the same method of microfabricated electrodes is used to determine the amount of white blood cells present in the sample. After these counted cells are lysed, the fluorescence from molecular beacons that have specifically bound to CD64 mRNA is measured with fluorescent microscopy. β -actin mRNA is utilized as a control in this section of the system due to its consistently normalized expression. The level of β -actin mRNA will be compared to the level of CD64 mRNA to determine the level of expression for CD64 mRNA.

Because each molecular beacon can be associated with a specific amount of fluorescence, the total amount of fluorescence can be utilized to quantify the total amount of CD64 mRNA in the leukocytes of the sample. The amount of CD64 mRNA and the total erythrocyte and leukocyte count are used to assess the progression and risk of sepsis for the patient.

In order to effectively assess the severity of BBCs and sepsis all of the quantified biological levels will be compared to a standard representing a healthy individual. However, for the first two phases of the microfluidic system, because tumor cells and tumor cell clusters are being measured, the simple presence of these cells is indicative of problems. Circulating tumor cell clusters are rare within circulation and are generally created from shedding tumor sites. Therefore the identification of CTCCs is a significant indicator of tumor sites within the patient. Individual CTCs are still very rare, but certainly more abundant than clusters. While the identification of CTCs in a blood sample doesn't necessitate a tumor, it certainly shows that the leukemia has progressed significantly and there is danger for metastasis. For the sepsis assessment and diagnosis section of the microfluidic system, the fluorescence of molecular beacons bound to CD64 mRNA is measured. The rates of fluorescence increase over time and the total fluorescence are representative of the CD64 protein expression within the system. The values of CD64 mRNA expression will be compared to levels of expression within healthy individuals in order to assess the progression and risk for sepsis.

One of the reasons we wanted our integrated diagnostic test to be composed of microfluidic chips is because they are inexpensive and easy to manufacture. After considering the different fabrication methods typically used to create a master mold for the fabrication of microfluidic devices, such as photolithography and 3D-printing, we decided that 3D printing was the most convenient method to use. Recent advancements in 3D-printing technologies now allow for highly complex microfluidic devices to be fabricated via single-step, rapid, and cost-effective protocols. Using 3D-printing for our mold fabrication method enabled us to rapidly design different device iterations in the development stage. Our original timeframe and budget for this project was \$1,500 and approximately 30 weeks. However, due to some necessary changes regarding the current health crisis and associated logistical difficulties, we were forced to drastically revise our project. These changes shortened our timeframe down to approximately 4

weeks and a budget of approximately \$250. Due to this, our project is largely literature based, with theoretical data formed from the papers that were the inspiration of our design.

Chapter 3: Background and Significance

3.1 Background and Motivation of Subject Matter

Cancer is a disease caused by genetic mutations that lead to excessive cell division, abnormal cell growth, and extended lifetime of cells. These genetic mutations cause large growths of cancer cells called tumors which interfere with natural bodily functions and commonly lead to death. These massive growths of cells can also spread to other parts of the body when cells from the tumor shed off of the cell and move around the body, as illustrated in **Figure 3.1**. Studies modeling the shedding of tumor cells in rats have shown that millions of these cells can break off of the tumor everyday. After breaking off of the primary tumor, the majority of these cells enter blood or lymphatic vessels and end up circulating around the body. Luckily, these cells do not survive very easily in the environment of circulating blood due to the lack of growth factors, physical stress, and the unfulfilled necessity of attaching to other cells. The majority of these cells do not survive the transportation process. However in some cases, these tumor cells will remain attached to each other and enter the bloodstream as a unit of many different cells. When tumor cells attach to each other in this manner, their likelihood of surviving transportation through the blood is significantly increased. This is because clusters can withstand shear forces of circulation better than single cells and are also resistant to immune attacks. The cells that do eventually exit the bloodstream and attach themselves elsewhere in the body can begin to form secondary tumors. This process is called metastasis, and the mobile cancer cells are called circulating tumor cells (CTCs). The diagnosis of cancer includes blood tests, x-rays, CT scans, and endoscopy however usually by the point that these tests have a definitive answer the disease has progressed significantly. In addition, metastasis is generally only discovered when tumors in other locations around the body begin to grow and are detected²¹.

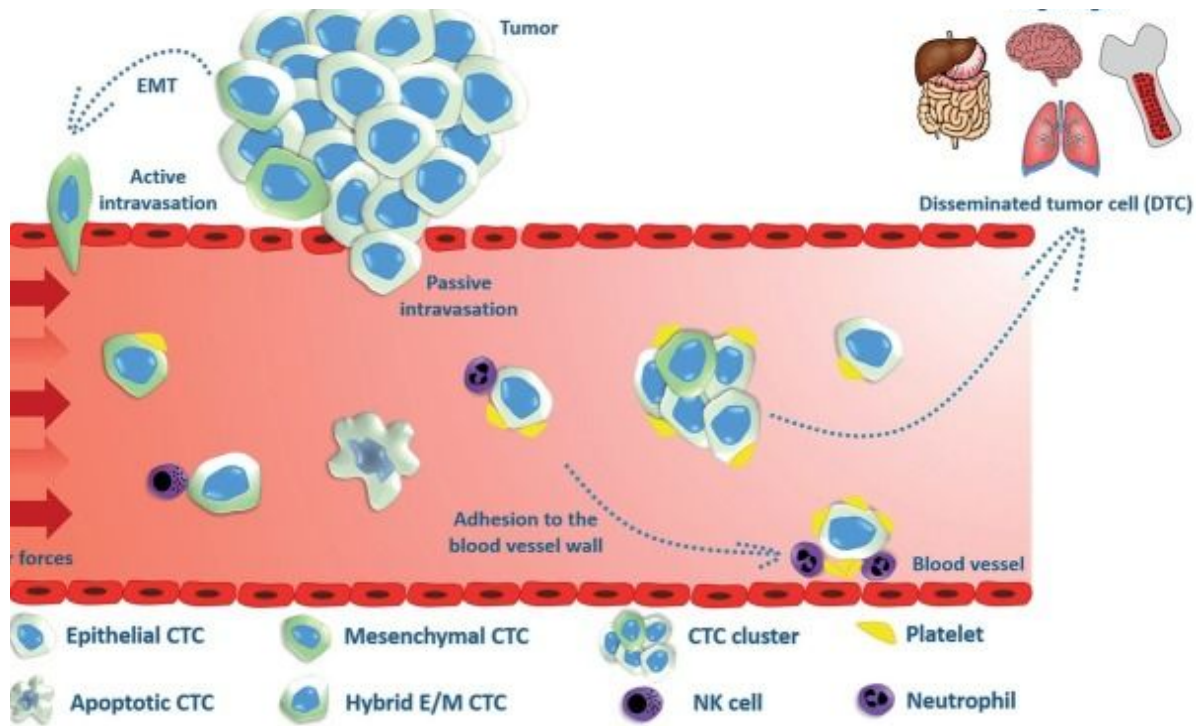


Figure 3.1: Cartoon sketch depicting CTC and CTCC mechanisms of movement in a blood vessel from a primary tumor. Adapted from Ref. F2

A novel way of diagnosing cancer and metastasis includes the separation and isolation of CTCs from a blood sample. Tests such as these have been found to have very high efficiencies of separating CTCs from blood samples. In addition, some of these methods have been very effective in separating low concentrations of CTCs in blood. Because the average concentration of CTCs in blood is roughly 5 cells per 10 mL, these methods have to be very effective and specific in order to achieve usable estimates.

There are various methods currently being used for the separation of CTCs from blood. These methods include positive and negative immunomagnetic enrichment, microfluidic immunocapture, and microfluidic filtration. Positive and negative immunomagnetic enrichment uses antibodies to separate CTCs from a whole blood sample. Positive immunomagnetic enrichment utilizes antibodies which tend to selectively bind to CTCs and separate them from the whole blood sample. There are various ways this method has been approached, yielding roughly

75%+ separation efficiency from various studies. Negative immunomagnetic enrichment also uses antibodies, however it attaches to other cells present in the sample only leaving CTCs within the mixture. Microfluidic immunocapture utilizes platinum electrodes for enumeration of CTCs and also flows the cells into a chamber where they are captured with heterogeneously bound antibodies. Lastly, is microfluidics for CTC filtration which utilizes the difference in physical properties of cells to filter them²¹.

3.2 Microfluidics

Microfluidics is the science of fluids and particles on the scale of micrometers, or 1×10^{-5} meters. Using microfluidics allows for reduced volumes of both samples and reagents, lower cost, higher sensitivity and portability, the ability to be automated, the ability to use size-based separation techniques, and the ability to precisely control the flow rate. One of the main ways of controlling flow through microfluidic channels comes through layering a control layer on top of the flow layer and filling it with water or buffer to stop the flow, much the same as stepping on a garden hose.

Inertial microfluidics is a simpler, more passive design that allows for precise manipulation and high throughput using a relatively simple structure. In inertial microfluidics, particles in a straight channel laterally migrate to different equilibrium positions, known as inertial migration. In fact, this phenomenon is particularly relevant to microfluidics, due to the particle size ratio to the dimensions of the channels. The inertial migration exists due to the counteraction of the shear gradient lift force and the wall lift force. Gradient lift force is from the curvature of the fluid velocity profile and how this curvature interacts with a particle, directing said particle towards the wall of the channel. Wall lift force is from the flow field interaction between the particle and the walls, repelling the particle from the wall.

Another major component of inertial microfluidics is secondary flow, where the fluid near the center of the channel has a higher momentum than that near the wall. This creates counter-rotating streams, which can create additional viscous drag forces on particles perpendicular to the main stream. These two components together allow for particle separation based on size, the foundation of this paper²².

3.3 Labyrinth Microfluidic Device for CTC Filtration

The design of this device was inspired by the Labyrinth in Greek mythology that was designed and built by Daedalus for King Minos of Crete to hold the Minotaur. The elaborate structure, with its numerous turns and corners, is perfect for size-based enrichment of CTCs by bulk depletion of hematopoietic cells using inertial microfluidics-based separation. CTCs are isolated from other blood cells in curved microfluidic devices by focusing different sized cells into different streamlines and collecting them into individual outlet channels. The inertial force focuses the particles, while the drag force from Dean flow causes particle migration away from the center of the channel²³.

As the particles are injected from the inlet of the channel, they immediately equilibrate into two broad bands near the longer channel wall under the influence of shear lift (F_S) and wall lift forces (F_W) acting vertically with respect to the channel height. When the flow velocity is relatively low, particles migrate laterally towards the center equilibrium due to a rotation lift force (F_R), forming two focusing streaks. As the flow velocity increases, the two streaks start to migrate towards the inner channel wall, followed by a single point focusing at a particular threshold due to the differential interplay between the net lift force (F_L) and the Dean drag force (F_D). Outer wall migration is induced as the flow velocity is increased above this threshold²⁴.

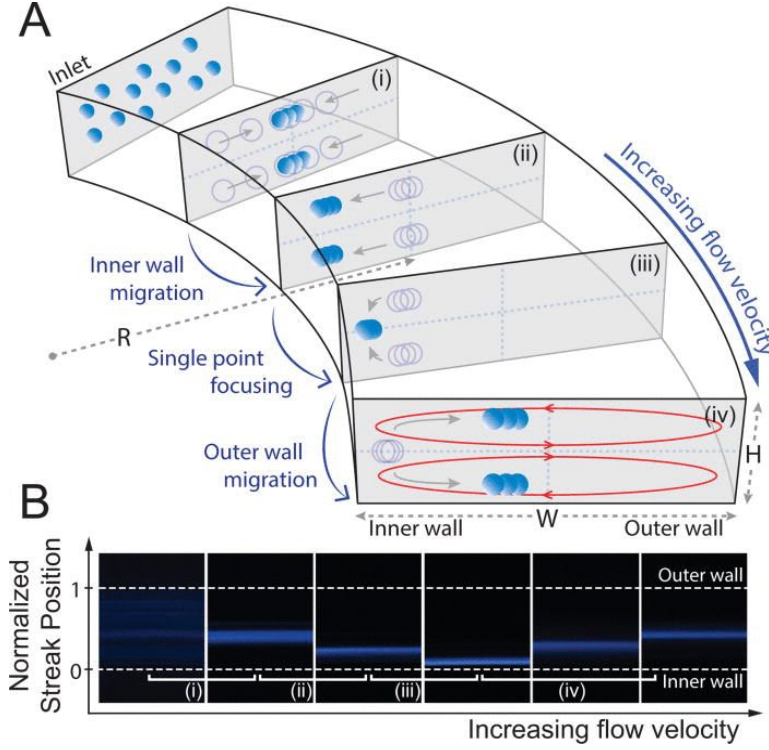


Figure 3.2: Visual representation of the Dean coupled inertial focusing profiles of particles in a curved low aspect ratio microchannel. Adapted from Ref. F3.

The relationship describing the magnitude of lift force (F_L) is the following:

$$F_L = \frac{\mu^2}{p} Re_p^2 f_c(Re_c, x_c), \quad \text{Eq. 3.1}$$

where Re_p is the particle Reynolds number, Re_c is the channel Reynolds number, and x_c is the position of the particle within the channel²⁴.

The expression for drag force (F_D) is given by:

$$F_D \sim pU_m^2 aD_h^2 r^{-1}, \quad \text{Eq. 3.2}$$

Where U_m is the maximum channel velocity, a is the particle diameter, D_h is the hydraulic diameter, and r is the radius of curvature of the channel²⁴.

Using these two equations, a new equilibrium position can be estimated from the ratio of F_L to F_D :

$$\frac{FL}{FD} = \frac{1}{\delta} \left(\frac{a}{Dh} \right)^3 \text{Re}_c^n, \quad (n < 0), \quad \text{Eq. 3.3}$$

Where δ is the curvature ratio²⁴,

$$\delta = \frac{Dh}{2r} \quad \text{Eq. 3.4}$$

It has been proposed that sharp curves enhance the focusing of smaller particles, which is the reason why our microfluidic device must contain curves with a high curvature ratio²⁵. What differentiates the labyrinth design from typical spiral designs is the fact that labyrinths have numerous sharp corners placed across the flow pattern. The sharper curvatures achieved by these corners enhance Dean forces to migrate particles toward their equilibrium positions, resulting in clean separated focusing of both large CTCs and small WBCs²⁴.

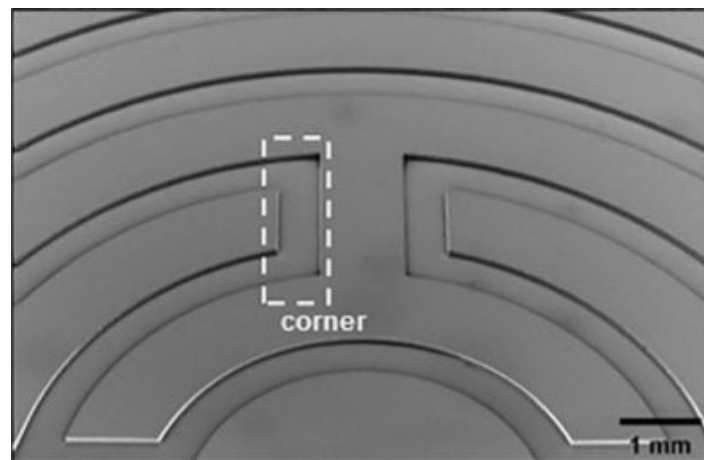


Figure 3.3: SEM image of sharp corners in Labyrinth that enhance Dean forces. Adapted from Ref. F4.

3.4 Sepsis and Mechanism of Propagation

Every year there are approximately 50 million cases of sepsis resulting in 11 million deaths. Sepsis presents with increased temperature, respiratory rate, CO₂ levels in blood and abnormal WBC count. Because these symptoms are common in many diseases diagnosing sepsis can be extremely challenging. In addition, the death rate for sepsis increases by 7.8%²⁵ every hour which means that prompt diagnosis is essential. Sepsis is an inflammatory autoimmune disease which is triggered by an infection or cancer. When pathogens or CTCs enter the blood, they are recognized by white blood cells and trigger an immune reaction. This immune reaction entails an exponential increase in the release of inflammatory chemokines and the recruitment of WBCs, causing significant tissue and organ damage. The cell that plays the largest role in this process is the neutrophil. The neutrophil is the most abundant white blood cell in the body which propagates inflammation through the degranulation of inflammatory chemokines. These chemokines attract other WBCs which continue the signal propagation. During this inflammatory process, neutrophils also release NETs (neutrophil extracellular traps) of chromatin and serine proteases with the biological intention of combating pathogens from spreading and replicating. However, excessive NET formation leads to intravascular coagulation and thrombosis. In addition the excessive amount of inflammatory chemokines can leak out of blood vessels and disrupt natural organ function. All of these factors, with their significantly increased abundance during sepsis, cause tissue damage and eventually organ failure.

The transmembrane protein utilized by neutrophils for the recognition of pathogens and CTCs is CD64. During sepsis, this protein is heavily upregulated as the cells attempt to increase their efficacy of pathogen recognition. CD64 is a commonly used biomarker for diagnosing sepsis because its expression increases as the severity of the disease worsens. During sepsis and similar inflammatory events, CD64 can be upregulated by a factor of 50 when compared to normal levels of the protein allowing for easily distinguishable diagnosis.

3.5 Molecular Beacons for the Enumeration of mRNA

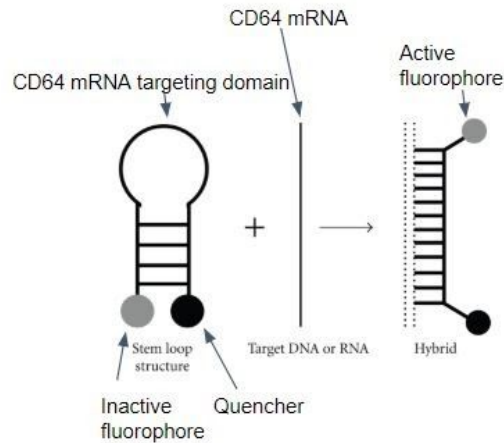


Figure 3.4: Sketch of the binding mechanism for molecular beacons, with the unbound beacon shown on the left and the bound beacons shown on the right.

Molecular beacons are a designed group of molecules commonly used in PCR and qPCR for the enumeration of DNA replicated in the procedure. A molecular beacon is composed of a fluorophore, a quencher, and an oligonucleotide strand as shown in Figure 3.5. The oligonucleotide is engineered to be antisense to the target DNA or mRNA so that it can bind specifically. When the oligonucleotide strand of the molecular beacon binds to the target molecule, the fluorophore becomes separated from the quencher molecule and becomes active. The active fluorophore will then fluoresce when light within a small range of wavelengths makes contact with it. This light excites electrons within the fluorophore which releases energy in the form of photons during de-excitation. The amount of released light from each fluorophore is then measured utilizing fluorescent microscopy to achieve a quantifiable amount of nucleotides within the solution.

Figure 3.5 represents a single fluorophore molecular beacon, however, recent developments have resulted in the creation of molecular beacons which have multiple fluorophores and quenchers resulting in a much stronger signal from the sample. The most commonly used multiple fluorophore molecular beacons are composed of three fluorophores

with their respective quenchers. These novel molecular beacons are able to produce fluorescence at rates up to 320 times larger than single fluorophore molecular beacons as shown in Figure 3.6.

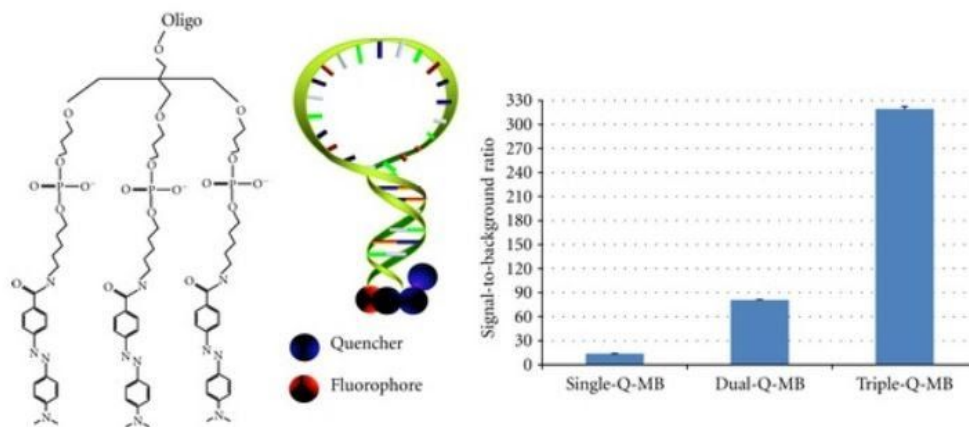


Figure 3.5: *Cartoon sketch of a triple fluorophore/quencher molecular beacon shown on the left, with a graph of the relative fluorescence of different molecular beacon designs on the right. Adapted from Ref. F5*

Chapter 4: Subsystems Overview

4.1 Pillar Chip

The cluster separation segment of the system occurs first because the flow rates which occur in the Labyrinth design are high enough to break up the clusters and lower the efficacy of the diagnosis. The mechanism for cluster separation is deterministic lateral displacement (DLD), in which groups of cells are horizontally displaced based upon size and asymmetry. The process occurs in two phases, both of which separate different sizes of clusters based on different qualities of the clusters. Due to the redundancy of Stage 2 isolating small CTCs as the labyrinth does the same, as well as the large time requirement (~6 hours), we decided to focus on Stage 1. Further information on Stage 2 can be found in Appendix section A2.

The first phase of the cluster separation design is focused on separating large clusters of cells (4+ grouped CTCs). This process works by flowing cells and clusters through many sets of slightly displaced rows of vertical pillars. Small clusters (<4 grouped CTCs) are able to simply weave through the rows of pillars and therefore move only vertically. Large clusters of cells,

however, are not able to weave through the pillars and are therefore displaced laterally as well as vertically as they move through the pillars of cells. This results in the small clusters and single CTCs being directly vertical of where they entered the chip and the large clusters being slightly laterally displaced. There are two outlets from the first phase of the chip, one directly below the blood entrance flow which collects small clusters and single CTCs, and one on the opposite side which collects large clusters.

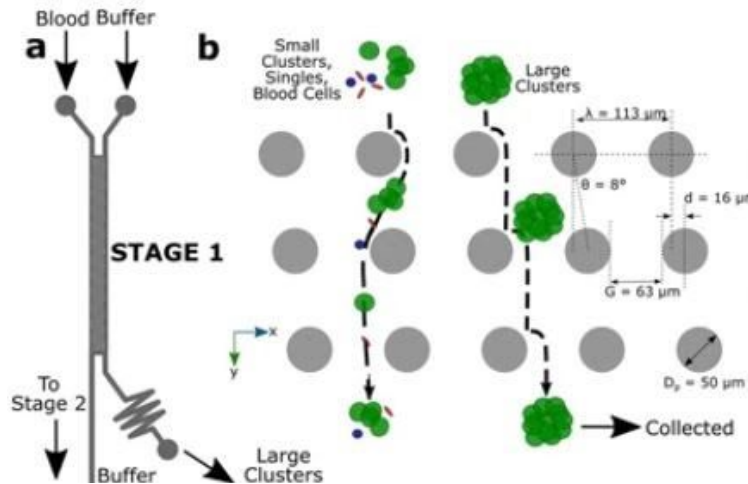


Figure 4.1: Cartoon sketch diagramming the mechanism of large cluster separation through deterministic lateral displacement. Adapted from Ref. F6

In order to separate large clusters, we decided to use the first section of the pillar chip design. As the cells enter the microfluidic system, the large clusters, which contain 4 or more cells, will be isolated through deterministic lateral displacement. These large clusters of cells will be forced to move diagonally through the system as they flow down through the rows of slightly offset pillars. The large clusters are collected on the right side of the chip, and will later be counted utilizing electrode cell counters. The small clusters and single cells will flow into the labyrinth section of the microfluidic system. The expected capture efficiency of this step is ~99%, and the flow rate being utilized is 16.6 ul/min. Initially we were planning on utilizing two stages of the pillar design to separate both large and small clusters but the run time for the chip

designed to separate small clusters was ~6 hours, and this took too long for our goal of having a < 2 hour runtime.

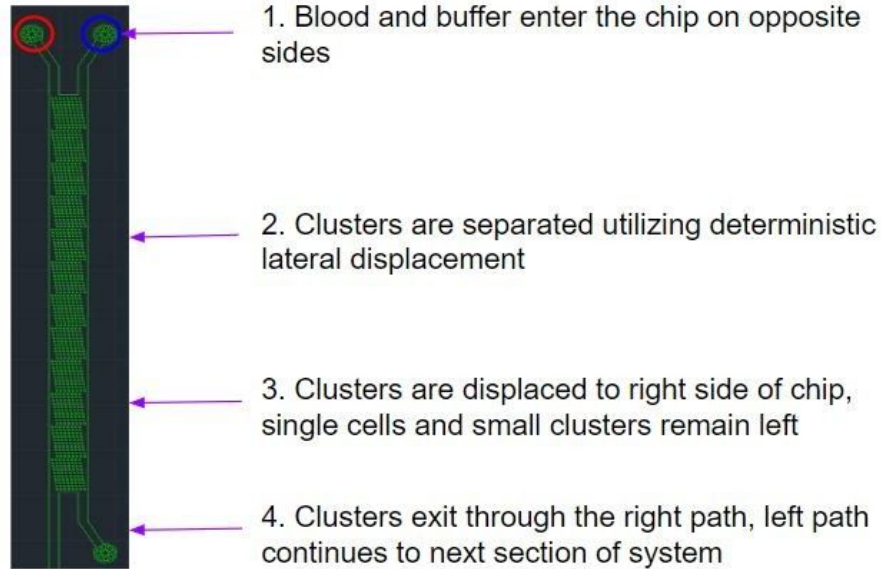


Figure 4.2: Cluster separation microfluidic chip AutoCAD design with blood and buffer entering through the top of the chip and separated clusters exiting on the bottom right.

4.2 Labyrinth Chip

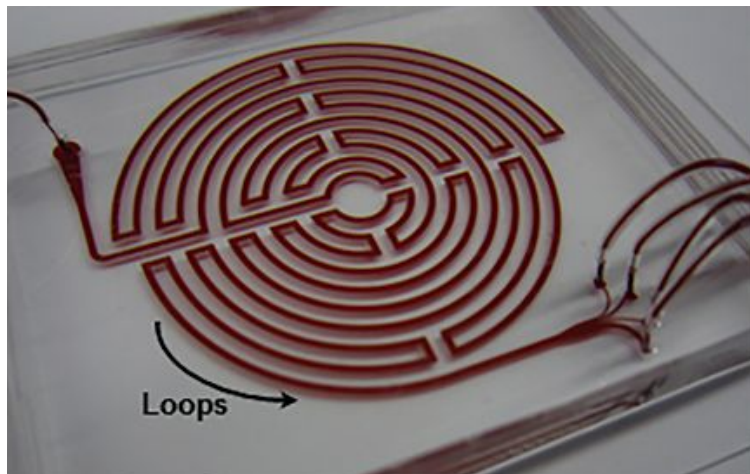


Figure 4.3: Long loops and sharp corners in Labyrinth result in clean and separated focusing of CTCs and small WBCs. Adapted from Ref. F4.

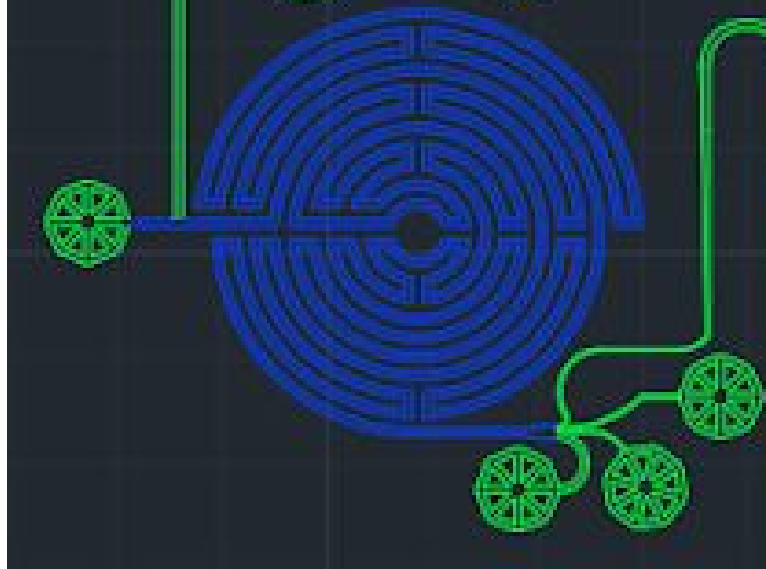


Figure 4.4: Labyrinth chip AutoCAD sketch with extra valve to pump buffer into the inlet. Color added to illustrate layer differentiation based on component height.

Now that the CTC clusters have been captured and the individual CTCs funneled into the inlet of the Labyrinth, we will have to increase the flow rate of the sample fluid from the CTC cluster separator that operates between 10-40 $\mu\text{L}/\text{min}$ to 1800–2600 $\mu\text{L}/\text{min}$. We will accomplish this by having a separate valve connected to the inlet injecting buffer at a flow rate of 1800-2600 $\mu\text{L}/\text{min}$, mixing with the sample fluid from the cluster separator. The reason we need to increase the flow rate so drastically is so that we generate enough inertial lift forces and Dean flow drag forces to focus and separate the cells by size. The inertial force focuses the cells in the channel, while the drag force from Dean flow causes the cells to migrate away from the center of the channel, resulting in size-based separation²⁷. Another benefit of adding the extra valve to the input of the valve is the fact that this valve could be used to pre-flow the device with 1% Pluronic acid solution (diluted in 1X PBS) at 100 $\mu\text{L}/\text{min}$ for 10 minutes, followed by an incubation time of 10 minutes²⁷. This step needs to be performed to prevent the cells from clotting on the channel walls²⁷. It could be performed as the blood sample is being processed through the cluster separator. The total channel length of the Labyrinth is 637 mm, it is 500 μm in width, 100 μm in height, and consists of 11 loops and 56 corners²⁷. The loops, which have a small curvature ratio, provide enough length of channel to achieve total focusing of cells and to

have the proper curvature for the separation of CTCs and blood cells²⁷. The 56 sharp right-angle corners, which have high curvature ratio, further enhance the focusing of smaller cells²⁷. The channel expands from a width of 500 μm to 1000 μm before diverting into four separate outlets to collect WBCs, CTCs, RBCs and other blood components²⁷. The outlet that contains the WBCs from the Labyrinth will be redirected to the CD64 positive neutrophil sepsis test.

The reason the authors wanted to develop a label-free isolation method is because many microfluidic devices rely on positive or negative selection to isolate CTCs, such as the immune-affinity capture method that utilizes antibodies to target molecules, such as the epithelial cell adhesion molecule (EpCAM), which are expressed exclusively on tumor cells²⁷. The drawback with these methods however, is that not all CTCs express EpCAM, and downstream single cell-analysis of captured CTCs can be challenging due to complex protocols that may interfere with RNA stability during the release step of CTCs from devices²⁷. They also wanted to address the drawbacks of using conventional curved channel or spiral channel microfluidic devices, because these devices are less successful at focusing small cells such as WBCs²⁷. Stronger mixing forces are required to move smaller cells to equilibrium positions and achieve better focusing of these particles, which can be proven by looking at the expression for the inertial lift force²⁷.

$$F_L = \frac{f_L \rho_f U_m^2 a_p^4}{D_h^2}$$

F_L = net inertial lift force
 $*f_L$ = lift coefficient
 ρ_f = fluid density
 U_m = maximum velocity
 a_p = diameter of particle
 D_h = hydraulic diameter of channel

Figure 4.5: Inertial lift force equation showing that the magnitude of the inertial lift force is proportional to the fourth power of particle diameter, which proves that smaller particles are harder to focus. Adapted from Ref. F7.

As you can see in Figure 4.5, the inertial lift force (F_L) is proportional to the fourth power of particle diameter (a_p), which means that smaller particles experience smaller inertial lift

forces. This is the reason why most spiral devices have to compromise for either low CTC recovery or low WBC removal as the smaller cells are not efficiently focused²⁷. However, by designing the Labyrinth with sharp corners across the flow pattern, the authors were able to enhance Dean forces to migrate particles toward their equilibrium positions while retaining clean separated focusing of both large CTCs and small WBCs²⁷. The percent recovery in outlet 1 during one of the control experiments was 91% for WBCs, and in outlet 2 the percent recovery was 92% for PANC-1 cells, 90% for H1650 cells, and 91% for MCF-7 cells to list a few cell lines²⁷.

A separate research team developed and optimized a novel Labyrinth microfluidic device to efficiently isolate CTCs from peripheral blood of Hepatocellular Carcinoma (HCC) patients²⁸. They made modifications to the original Labyrinth and increased the height of the channel to 110 μm . This modification increased the Dean force effect, allowing the cells to equilibrate at similar focusing positions at lower flow velocities, which reduced the overall shear stress acting on the CTCs during separation. The Labyrinth device has an inlet to inject the sample, and four outlets. Outlet 1 collects WBCs, Outlet 2 collects CTCs, and Outlets 3 and 4 were included to reduce the sample fluid volume after cell separation and collection. Spike-in experiments to determine the recovery rate of CTCs in Outlet 2, at the determined optimal flow rate of 2000 $\mu\text{L}/\text{min}$, revealed a recovery rate of 91.17% and 95.69% for Hep 3B and Hep G2 cells respectively after considering only the cells with a size above the cut-off cell diameter entering the outlet²⁸. The WBC depletion rate at this optimal flow rate was determined to be $97.66 \pm 0.53\%$. After optimizing the flow rate of the Labyrinth with spike-in experiments, the researchers tested the device with peripheral blood from HCC patients, and identified CTCs in 88.1% of the patients over different tumor stages²⁸. Interestingly, they also found that 55% of the patients had the presence of circulating tumor microemboli (CTM), sometimes referred to as circulating tumor cell clusters (CTCCs)²⁸.

While we didn't make drastic modifications to the Labyrinth device, mainly because it is already highly efficient at separating CTCs and WBCs, the integration of the Labyrinth into a full metastasis test that also detects CTC clusters and CD64 positive neutrophils will have important value for its clinical application.

4.3 CD64 mRNA Expression Chip

The sepsis diagnosis system within our senior design project is designed to quickly and effectively quantify the expression of the CD64 transmembrane protein for sepsis diagnosis. This step occurs directly after the CTC separation that takes place within the labyrinth design. This process occurs in 5 steps, including the enumeration of leukocytes and erythrocytes, the lysing of the patient's leukocytes, the mixing and binding of the Molecular Beacons to CD64 mRNA and β -actin mRNA, the fluorescent microscopy of the bound CD64 mRNA, and finally the data interpretation. After the CTC separation within the labyrinth chip, the remaining cells will primarily be composed of leukocytes. These leukocytes include neutrophils and monocytes, both of which present the CD64 transmembrane protein. The mRNA that encodes the CD64 protein can be quantified in order to determine total CD64 expression and diagnose the severity of sepsis.

In order for efficient access to this mRNA, which is located in the cytoplasm, the leukocytes will be lysed with a lysing buffer composed of water, NH_4Cl , KHCO_3 , and Tetrasodium EDTA²⁹. Initially, there was a concern as to the availability of the CD64 mRNA however certain studies have shown that there is a significant upregulation in CD64 mRNA during events of inflammation within the body³⁰. These significantly increased levels of mRNA will not only be numerous enough to be imaged, but their levels of upregulation will provide a significant amount of information in regards to the severity of the inflammation.

The lysed cells then enter the rotary chip. As they enter the rotary chip they will be mixed with the engineered molecular beacons. The engineered molecular beacons will utilize MPQ3 as the fluorophores in addition to a triple quencher/fluorophore site in order to receive a stronger signal from the labeled mRNA³¹. This MPQ3 triple fluorophore site has been shown to produce a fluorescence that is significantly stronger than single fluorophore/quencher sites. These fluorophores will only become active after the oligonucleotide sequence has specifically bound to the CD64 mRNA. In addition to the CD64 targeted molecular beacons, molecular beacons targeting β -actin will be used. These molecular beacons will utilize a similar triple quencher/fluorophore site, however BHQ2 will be used instead of MPQ3 in order to differentiate between the fluorescence from each mRNA. These β -actin mRNA targeting molecular beacons

are utilized to determine a control level of mRNA expression and will provide a non-upregulated point of comparison to determine the level of expression for CD64 mRNA. As shown in Figure 4.4, the molecular beacons and the lysed WBCs will enter the chip. In order to facilitate the mixing and proper binding of the solutions, oscillating pressures within a circular path are applied.

From this point on fluorescent microscopy is being applied to the mixture and the photons produced after MPQ3 and BHQ2 excitation will be measured. Because each fluorescent beacon corresponds to a specific amount of reflected light, the total amount of reflected light can be used as a method of quantification for the labeled CD64 and β -actin mRNA. After the mixture flows out of the mixing circular path, it enters a reservoir which is also under fluorescent microscopy. The mixture that enters this reservoir will remain there as the rest of the molecular beacons are mixed.

Finally, the fluorescence data must be interpreted. The MPQ3 fluorophores and the BHQ2 fluorophores will fluoresce with light that has wavelengths of 485nm and 600nm respectively. The released photons from each of these fluorophores will also vary in wavelength. The measured levels of fluorescence for each of the fluorophores will then be compared to get quantitative amounts of expression for both CD64 mRNA and β -actin mRNA. These expression levels will then be compared in order to determine the severity and stage of sepsis. In inflammatory diseases, CD64 expression can increase up to a factor of 50. Therefore, depending on the difference of fluorescence magnitude of each wavelength, the severity of sepsis can be quantified³⁰. Based upon the increase in fluorescence over time and the total fluorescence, total CD64 mRNA can also initially be estimated and later fully quantified. Depending upon the rate of increase in fluorescence it is possible to estimate the total amount of CD64 mRNA in the sample. If the measured fluorescence is increasing very quickly, it is indicative of a large amount of CD64 mRNA in the sample. While this estimation may not be quantitative, it can save a significant amount of time during sepsis diagnosis and potentially allow the early administration of treatment for sepsis which can potentially save the patient's life.

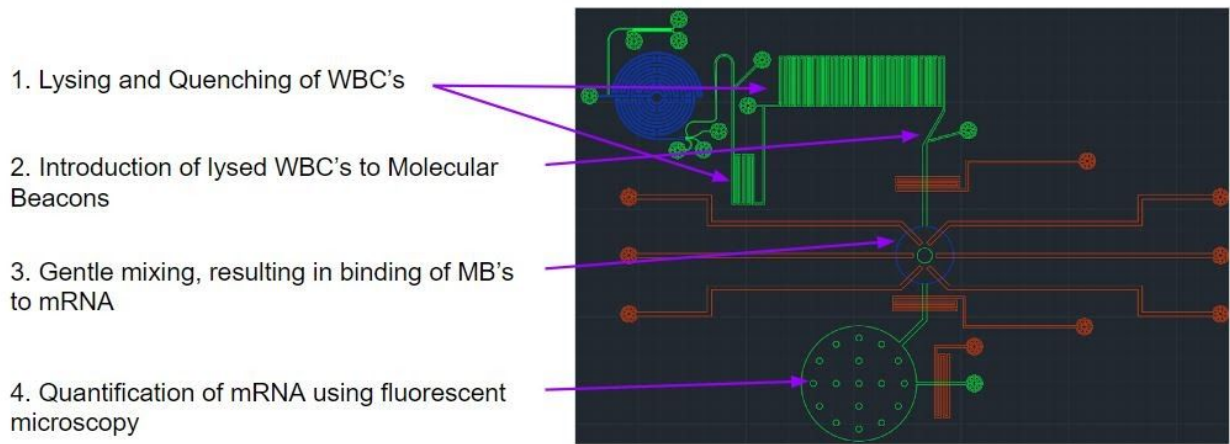


Figure 4.6: AutoCAD diagram of sepsis assessment in the microfluidic system with lysing and quenching pictured on the top in green, the mixing channels pictured in the middle in red, and the imaging reservoir pictured on the bottom in green.

Chapter 5: System Integration

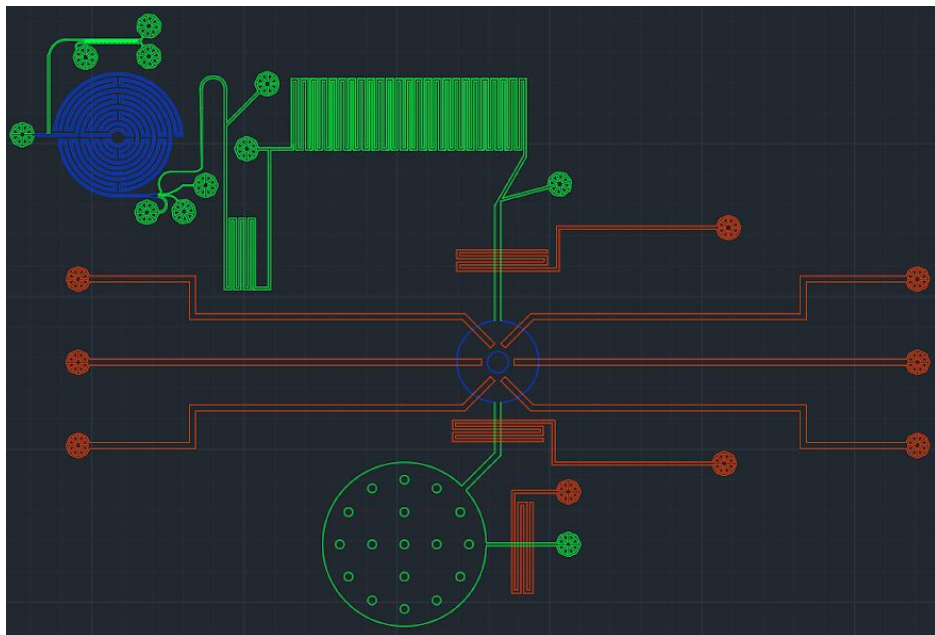


Figure 5.1: AutoCAD design showing full system integration of the various components and control layer based chamber isolation.

For our device, we have several different components working together to analyze different common cancer complications. Once we finalized designs for each of these individual components, the next major step was putting all of them together. This came with a few additional challenges, in that not all of the components were of similar size. Given that the Labyrinth was the largest of the components, we had to resize some of the components to be able to hold the same volume of blood sample as the Labyrinth. We resized the components that were not size dependent for their operation, specifically the sepsis fluorescence device. Once we were able to properly resize all of the components, our final device size was 23.5 cm x 18.7 cm x 110 μm (blue layer) or 90 μm (green/red layer). While we considered different component arrangements for our device, we decided on starting with the cluster device, as the clusters are the most fragile biological component that we are measuring. Additionally, we decided that the sepsis analyzer should be last, given that it lyses the WBCs, so they cannot be used for other tests. If we put the sepsis analyzer leading directly from the WBC output of the Labyrinth, we would also be able to drastically reduce the sample size by only using the necessary blood components. This leads us to our next major issue.

Once we had all of the components put together, we found that the overall time it would take for a 7.5 mL sample to run through was 17.03 hours, or 17 hours and 2 minutes. This was far too long, so we looked for ways to reduce the time for our test. Our first major solution was to utilize the Labyrinth's ability to separate blood components and only run the WBCs through the sepsis analyzer. WBCs take up less than 1% of blood, which greatly reduced the test volume for this component, as mentioned above. This alone reduced our full testing time to 8.35 hours, or 8 hours and 21 minutes. This was still not good enough for us, so we decided to remove the second stage of the cluster separator that separates small CTCCs. Given that it only had approximately 65.5% efficiency in removing small CTCCs, and the Labyrinth has also been observed to have the ability to separate small CTCCs, we decided to remove it, which reduced the total test time further to 1.86 hours, or 1 hour and 52 minutes. While our goal was for the test to take less than two hours, we could not find any other way to reduce the test time without significantly affecting efficiency. For example, reducing the overall test volume would reduce our time by approximately 8 minutes per 0.5 mL, but given the rarity of CTCs and CTCCs, we

felt that reducing the volume could negatively impact our test's efficiency. We are satisfied with our testing time because it is significantly better than that of a standard blood culture test to diagnose sepsis, which can take several days to send to a lab, process, and receive the results.

Once the time issue was resolved, and the design was completed, we were able to resolve our next issue, which was the fact that the different components of our device required varying flow rates and test volumes. Test volumes were easy to fix, by sizing up the sepsis analyzer to allow for a larger sample to be analyzed, and allowing for more time for the cluster separator, which was factored into the above calculations. We were able to resolve the flow rate issue by adding buffer valves to inject additional buffer at higher rates of flow leading into the Labyrinth (highest flow rate), and increase the microfluidic pipeline diameter leading into the sepsis analyzer (lowest flow rate), which was also slowed due to the small percentage of the total volume being comprised of WBCs.

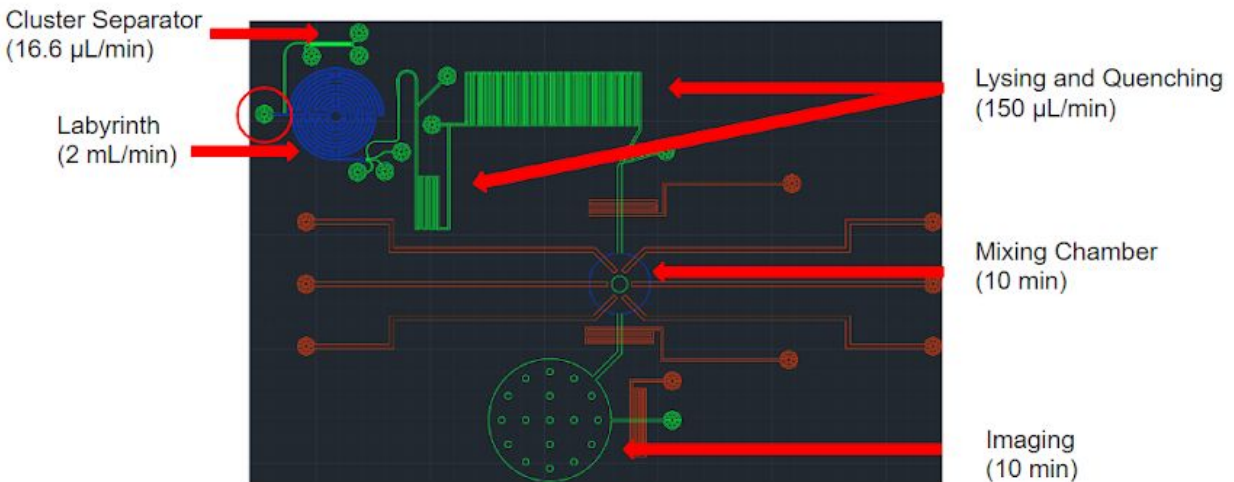


Figure 5.2: Different labeled subsections with flow rates or stop times, with highlighted valve for Labyrinth flow rate increase.

We were then able to add components to the full test, however due to the current health crisis, we were not able to practically incorporate these components, so this section will be largely theoretical. The main components to be added were electrode-based counters to read the outputs for each component. They would be two electrodes with a current between them, and when a biological component passes between them, there is a noticeable impedance correlating

to what and how much is passing through. We would place these counters at the end of stage 1 of the cluster separator to count large CTCCs, and at the end of the Labyrinth to count blood components (specifically WBC and platelets, for leukemia/lymphoma, and severe sepsis, respectively). We would set thresholds within the code for these counters correlating to dangerous levels for each component. Any of the following levels would trigger a “yellow” warning, correlating to low risk: WBC < 30,000,000 or > 90,000,000 for sepsis³², WBC < 4,500,000 for lymphoma³³, WBC > 7,500,00,000 for leukemia³⁴, CTC > 0 for metastasis, or CD64 mRNA expression >20 fold difference when compared to patient control for sepsis (discussed later). A “red” warning would be triggered by any of the following levels: platelet count < 750,000 for severe sepsis³², or CTCC > 0 for severe metastasis. These numbers correlate to a 7.5 mL blood sample, and will vary depending on how much blood is tested. We would also add a fluorescent imaging device and associated program to automatically count the mRNA biomarker in the WBCs for sepsis. The rest of the components that we would need to add would facilitate automation of our device, including a valve automation program to create different flow rates for the necessary input chemicals and buffer, a needle array for the input/output valves, and associated holding tanks for input, output, buffer, and all necessary chemicals.

Chapter 6: Results

Because we were unable to perform our own experiment due to the unavailability of lab space, we utilized example data from articles we explored in our literature review. Due to the multifaceted nature of our device, there was no single study which we could draw all of our hypothetical data from. Instead, we utilized data from several different articles which was applicable to specific sections of our microfluidic system and interpreted it as we would if the data had been collected from our device.

6.1 Hypothetical Pillar Data³⁵

The utilized cluster data was taken from a study titled “Quantitative flow cytometric identification of aberrant T cell clusters in erythrodermic cutaneous T cell lymphoma.” The

purpose of the study was to perform survival analysis of patients with stage III/IV lymphoma to determine what effect clusters had on death rate. The study utilized 61 blood samples from 28 patients with late stage lymphoma and analyzed them for the presence of clusters by utilizing flow cytometry. Out of the 28 patients, 17 (61%) presented with a significant amount of aberrant clusters. In addition, the study found a significant association between aberrant cluster presence and increased death rate at a 95% confidence interval ($P = .0227$).

In the context of our microfluidic system, having 61% of patients presenting with aberrant clusters is very high. The target population of our microfluidic system is not patients who are already in late stages of lymphoma or leukemia, instead our device is targeted towards the at risk population and early stage cancer patients. Therefore, we would expect to see a significantly lower percentage of patients with circulating tumor cell clusters. The presence of circulating tumor clusters in a patient indicates that either metastasis has already occurred or there is a very high danger of successful metastasis. This information could be essential to a physician when prescribing treatment to a patient due to the fact that cluster presence indicates a severity of cancer which can not be shown through normal testing. In addition, cluster presence has been shown to have a significant association with an increase in death rate. Therefore, after the presence of clusters is detected, the severity of chemotherapy and associated drugs should be increased in response.

6.2 Hypothetical Labyrinth Data³⁶

The only study with data relevant to the Labyrinth section of our device is “New Labyrinth Microfluidic Device Detects Circulating Tumor Cells Expressing Cancer Stem Cell Marker and Circulating Tumor Microemboli in Hepatocellular Carcinoma.” The research team evaluated the total number of CTCs in blood samples from 42 HCC patients and 5 non-HCC healthy control subjects. According to standard AJCC TNM staging, 26 (61.9%) of the HCC patients were stage II or above, and multiple nodules were observed in 19 (45.2%) of the HCC patients. It was also evident from the radiographs of 10 of the patients (23.8%) that macrovascular invasion was present. After gathering this information from the patients, the researchers finally processed the blood samples of the HCC and control patients to see if there

was any correlation between the presence of CTCs/CTCCs and tumor metastasis. They used IF analysis to identify CTCs as CD45 negative and HCC marker positive cells with intact nuclei stained by DAPI. In the HCC patients, they detected anywhere between 0.4 to 8.7 CTCs/mL (mean = 3.36 ± 0.31 CTC/ml, n = 42), which was significantly higher than that from the healthy control patients ((mean = 0.53 ± 0.1 CTC/ml, n = 5) (p = 0.0001). It was also observed that patients with higher TNM stages, stages II-IV, had higher numbers of CTCs (3.73 CTCs/mL, n = 26) than lower TNM stage patients, stages 0-I (2.76 CTCs/mL, n = 16). Unfortunately, the difference in CTC numbers between the two cohorts was not statistically significant (p = 0.1258). Of the 10 patients who presented with macrovascular invasion, 100% of them were positive for CTCs. In the other 32 patients that did not present with macrovascular invasion, 84.4% had detectable CTCs. The data did not reach statistical significance because there was a limited number of patients with macrovascular invasion (p = 0.1829). CTM were also observed among the CTCs isolated from the HCC patients, with numbers ranging from 0 to 1.29 CTM/mL in all stages of HCC (mean = 0.19 ± 0.04 , n = 42). CTM were not observed in any non-HCC control subjects (n = 5). Supporting the fact that CTM are more metastatic than single CTCs, the researchers found that the number of CTM was significantly higher in more advanced TNM stage patients (mean = 0.26 ± 0.06 n = 26) than that of early TNM stage patients (mean = 0.08 ± 0.03 , n = 16) (p = 0.0172).

The most important takeaway from this data is that the number of CTCs and CTM was higher in more advanced TNM stages, which suggests that there is a link between these cancer cells and tumor metastasis. The Labyrinth data is important for our application because one of the main types of solid-body tumor that blood based cancers can present with is leptomeningeal metastasis. Our hope is that our device would be able to detect this metastasis in the early stages, improving patient survival. Additionally, Stage 3 cancer associated with solid-body tumors can metastasize into lymph nodes near the site of the original tumor. This lymph node metastasis is otherwise known as lymphoma. Our goal with this device is to be able to detect metastasis from solid-body tumors before it has the opportunity to reach the lymph nodes and turn into lymphoma.

In our case, data collection for CTCs and small CTC clusters would have involved flowing in the sample from the pillar chip, which at this point would have already separated large clusters from single CTCs, small clusters, and WBCs, into the inlet of the Labyrinth. After collecting the single CTCs and small clusters from outlet 2, we could stain the cells and perform fluorescent microscopy to take images of the cells as seen in **Figure 6.1** and **Figure 6.2**, allowing for a CTC and cluster count, differentiation between CTCs and small clusters, and visualization of cell morphology. Several studies have already confirmed that the number of CTCs as well as their phenotypic changes in response to treatment can provide useful information to oncologists for individual treatment. Higher CTC counts often correlate with lower overall survival rates, and phenotypic changes can indicate acquired drug resistance.

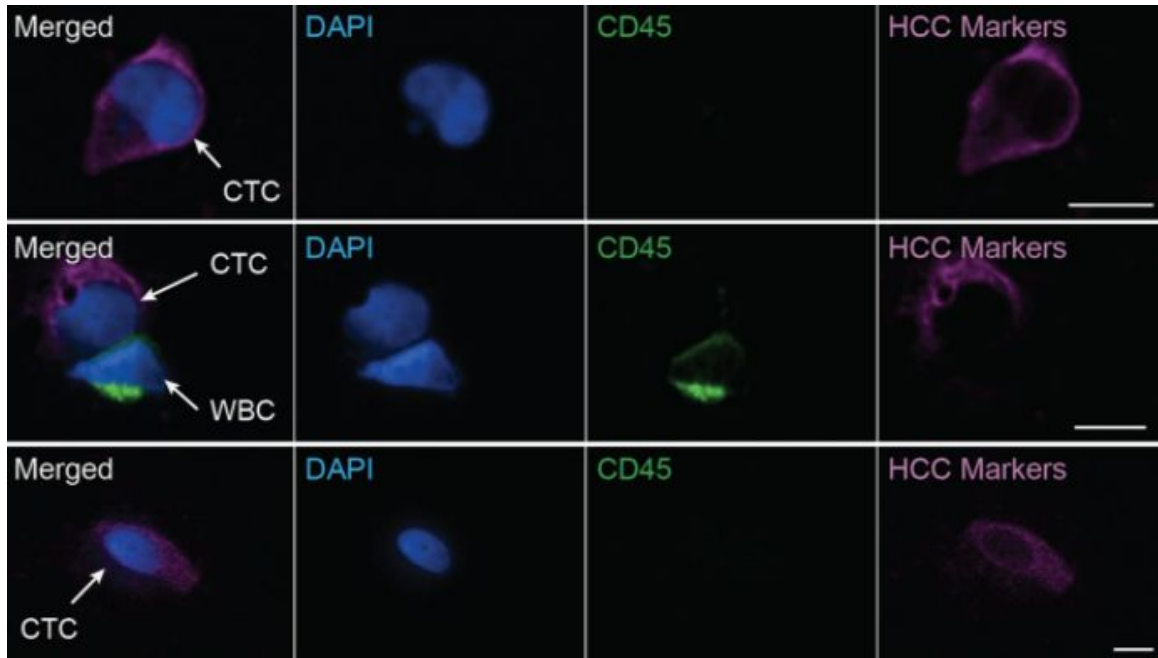


Figure 6.1: Stained CTCs isolated from HCC patients. Adapted from Ref. F8.

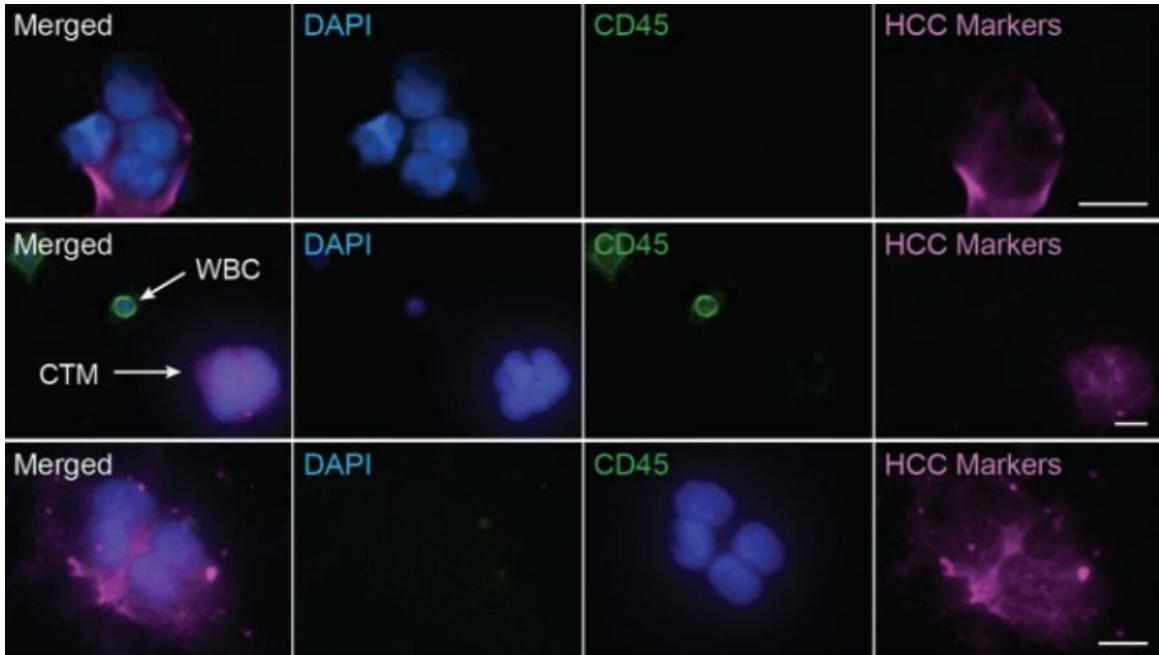


Figure 6.2: Stained CTM isolated from HCC patients. Adapted from Ref. F8

6.3 Hypothetical Sepsis Assessment Data³⁷

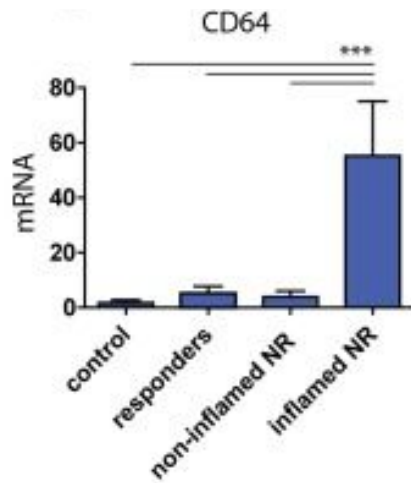


Figure 6.3 Graph representing the difference in expression of β -actin mRNA, labeled as control, and CD64 mRNA, labeled as inflamed NR, in inflamed and non- inflamed tissue.

Adapted from Ref. F9

The utilized sepsis analysis data was taken from a study titled “Fc gamma receptor CD64 modulates the inhibitory activity of infliximab”. This study was focused on assessing the efficacy of anti-TNF antibodies on inflamed tissue. Their method of assessing and determining why the drug may not be working as expected included the measurement of CD64 mRNA in inflamed tissue. The researchers hypothesized that the excessive CD64 expression counteracted the anti-inflammatory mechanism of anti-TNF antibodies. During their experiment, they measured CD64 mRNA expression compared against β -actin mRNA which was utilized as their control. The study found that during significant inflammation, CD64 mRNA is expressed more than β -actin mRNA by a factor of >50 as shown in **Figure 6.3** ($P < .001$). This comparison of expression between CD64 mRNA and β -actin mRNA which resulted in such a significant difference in expression is similar to the data we would expect to achieve from our sepsis analysis system. Such an increased expression of CD64 mRNA is indicative of severe inflammation, and a similar upregulation would be observed in sepsis. For our testing, upregulation of CD64 mRNA greater than β -actin mRNA by a factor of >20 would be indicative of sepsis and require immediate treatment. In addition, this study found that the upregulation of CD64 mRNA resulted in decreased efficacy of anti-inflammatory drugs. This finding solidifies the necessity of early sepsis diagnosis because as the disease progresses, it not only becomes more deadly at a high rate, but it also becomes more challenging to treat. For this reason, we decreased the testing time of our microfluidic system by as much as possible so as to gain an understanding of the patient's situation before the disease progresses excessively.

Chapter 7: Engineering Standards

7.1 Manufacturability

Due to the microfluidic nature of this device, the manufacturing process is significantly facilitated. The majority of this device can be created by 3D printing molds of each section and then filling them with PDMS to create the actual microfluidic device. The molds will be created based upon the height of each microfluidic section, then after filling, each section with varying height will be stacked in order to create the full microfluidic system. Some parts of the system,

however, can not be 3D printed and will instead be bought separately and then introduced to the system. These parts include the electrode cell counters, the fluorescence imaging device, and extra microfluidic parts such as pipettes and pumps. In addition, every part of the system making contact with the blood is biologically inert and will be sterilized prior to introduction of blood.

7.2 Environmental/Sustainability

Given that our integrated liquid biopsy microfluidic chip is only 23.5 cm x 18.7 cm x 200 μm in length, width, and height respectively, it does not produce as much waste as standard label-based CTC capture protocols or sepsis blood culture tests. Laboratories and healthcare facilities already contribute greatly to the plastic waste generated with single-use plastic materials such as pipettes, culture flasks, test tubes, etc., so we did not want our device to add too much to the waste burden. Additionally, since our device uses very small volumes of liquids, it cuts down on the chemical reagents that need to be properly collected and disposed of in hazardous waste facilities.

7.3 Economic/Social/Political

Mass-manufacturing of our device would help drive down the cost of a single unit, and as a result would make it more accessible to the communities that need it the most, mostly children in developing countries. According to patient case records of children with acute lymphoblastic leukemia (ALL) from a medical center in northern India, sepsis (53.3%) and bleeding (15.7%) were the most common causes of mortality in the 128 deaths that were recorded (24% death rate)³⁸. When you contrast this death rate to the 2.6% death rate reported from an analysis of the causes of death, other than resistant disease or relapse, in 875 children with ALL treated on 3 different Dutch Childhood Oncology Group ALL protocols, the difference in death rates is astonishing. Survival rates in childhood ALL in developing countries with limited resources are inferior because of infection-related toxic deaths, a higher incidence of relapse, default of therapy, and loss to follow-up. The main demographic we want our device to serve is children in developing countries, because as noted above, survival rates in childhood ALL in developing

countries is lower than in developed countries because of the lack of resources. Our device will be readily available to these countries because it will be easy and cheap to manufacture, as well as user friendly, eliminating the need for highly trained staff to perform other diagnostic tests such as flow cytometry or FACS to observe neutrophil CD64 expression. Additionally, our device integrates CTC and CTC cluster capture to provide additional prognostic information about the patient's cancer status. While our main target demographic is children in developing countries, our device will also be available to any pediatric patient with blood-based cancer.

Ethical/Health and Safety

As with any prognostic medical device, if an incorrect result is given, this kind of information could place a heavy burden on the pediatric patient's mental health, as well as the child's family members. Since our main demographic is children, who are not autonomous and need a legal guardian to make decisions for them, huge responsibility is placed on the legal guardian to decide if they think it is appropriate to run the prognostic test.

Chapter 8: Summary and Conclusion

Our work has resulted in the design of a microfluidic device which can process 7.5 mL of a patient's blood and analyze it for the assessment of leukemia progression, as well as common leukemia complications, such as metastasis (leukemic or solid-body tumor) and sepsis. Our device does this by isolating circulating tumor cells and circulating tumor cell clusters for solid-body tumor metastasis diagnosis, quantifying mRNA levels for sepsis diagnosis, platelet count for severe sepsis diagnosis, and WBC levels for leukemia progression and lymphoma metastasis diagnosis.

Our device completes these tasks in three distinct and continuous microfluidic stages. The first stage utilizes a staggered pillar design to isolate circulating tumor cell clusters for metastasis assessment and future analysis. The next stage utilizes a labyrinth design to separate smaller CTCCs, individual CTCs, and blood components for further metastatic assessment. The

designs for these stages were found in our literature review and then edited in order to achieve the function we desired in our microfluidic device. The third stage of the microfluidic system is of our own design and utilizes components commonly found in qPCR experiments. In addition, the full processing of blood will be completed in less than two hours which is significantly shorter than modern tests for these diseases. Once the test has completed, the data will include CTC and CTCC counts in addition to CD64 mRNA quantification, platelet count, and WBC count to compare against established baselines and pre-set trigger thresholds based on the various complications the patient might be facing. This data can be used to assess the severity and presence of leukemia, lymphoma, cancer metastasis, and sepsis.

We designed our device to overcome several shortcomings of previous technologies, such as a misdiagnosis risk and testing time. Given that both sepsis and leukemia present with high white blood cell count, it is very important to have a proper diagnostic distinction between the diseases for proper treatment. Our device allows for facilitated distinction between leukemia and sepsis because it allows for CD64 quantification, which is unique to sepsis, as opposed to the standard WBC test. Additionally, the average time of non-emergency complete blood tests is 4.5 hours, which is much too long for an effective test for sepsis. The death rate of sepsis increases by 7.8% every hour which means that the test must be completed quickly so that treatment can begin. Our device not only prevents the common misdiagnosis of sepsis but also provides the quantification of a biomarker which is indicative of sepsis severity in half the time of a normal blood test.

Our project unfortunately had several limitations because our team was unable to physically create and test our device as a result of COVID-19. This and several other unexpected problems forced us to redesign our project several times and limited the amount of time we had to work on the project. In addition, we were limited by the availability of data that was applicable to our work. Because we could not test our device, the data we utilized for our project had to be taken from outside sources. This was problematic because there are not a significant amount of studies done that result in data similar to the data we would be achieving from our device. We were instead forced to utilize data from studies and fit them to our work as best as possible.

We believe that this project will contribute to the medical community by providing a faster, smaller, and simpler device to test for cancer complications. We believe that we are also contributing to the community of Santa Clara University by helping those less fortunate by creating a device primarily for the benefit of a pediatric demographic, that also can be used by those in developing countries. Finally, we are contributing to our group members by allowing us to have an opportunity to learn new things in the world of medical device bioengineering, as well as prevent or reduce severity of medical complications that we may have a personal connection with.

If a future group were to pick up our project we would recommend that they work on increasing the efficiency of the device. This includes reducing the total run time of the device and potentially increasing the quality of data received. In addition, we recommend utilizing some sort of electric field within the reservoir chamber to focus the bound mRNA at the top resulting in more accurate data for sepsis assessment. The main focus of future work, however, should be actually building and testing the device, as well as writing the necessary programming functions for automation of the system. This is essential because all of our work is hypothetical until the device is actually built and tested, and there could be unforeseen issues with the design that would only become known during a practical test.

APPENDIX

A.1 Additional Information: Electrode Cell Counter

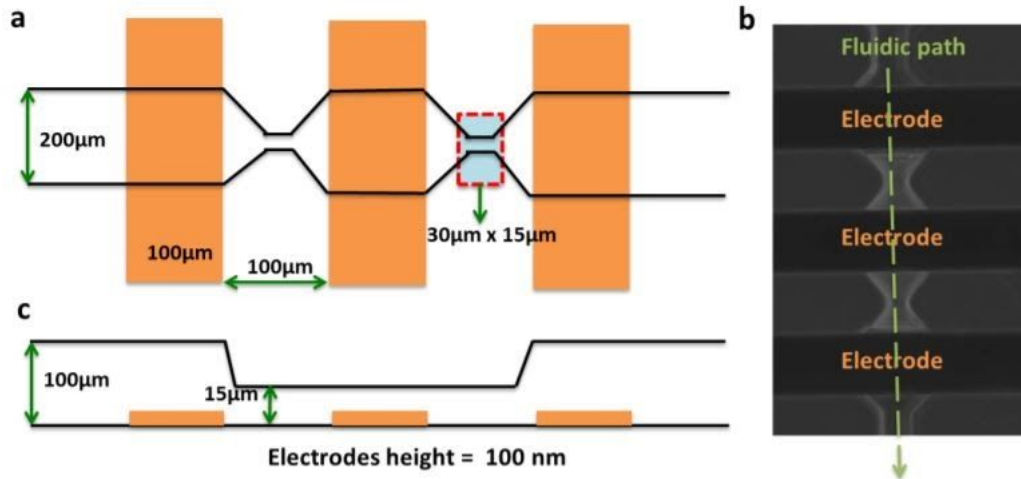


Figure A.1 Electrode Cell Counter with a top-down view pictured in A, and a side view pictured in C. The Section titled B shows a picture of the electrode cell counter from the side with the current represented in white. Adapted from reference A1.

Figure A.5 represents an electrode cell counter which utilizes disruptions of current in order to count cells as they pass between electrodes. This mechanism of cell measurement is known as the coulter principle. Between the electrodes, there is a path of current which gets disrupted when cells pass through it. The disruptions in current are dependent on the size of the cells which pass between the electrodes allowing for cell quantity and size estimation. The relative disruptions in current are analyzed through a neural network in order to create these estimations. This allows for distinguishability between different cell types and quantification of clustered cells as they pass through the system.

A.2 Additional Information: CTCC Separator Stage 2

The second phase of the cluster separation section of the system utilizes deterministic lateral displacement in order to separate small clusters of CTCs from single CTCs. The process begins as the small tumor clusters and single CTCs flow from the first stage of the chip. The

DLD of this stage works similarly to the first stage of the cluster separation process, however, the pillars are shaped differently and have different gap sizing. The clusters and single CTCs enter at the top of the chip and flow downwards through the rows of displaced pillars. Single CTCs are easily able to weave in between the pillars, the small clusters, however, do not do this. The pillars are asymmetrically shaped with a circular indent on the right side. This indent alters the flow of the buffer and cells as it passes by the pillars forcing the small clusters of CTCs to rotate as they flow past the pillars. This rotation forces the small clusters to exit the indent and move downwards at a different angle than the single CTCs. The exiting angle of movement for the small clusters has them move straight downwards rather than horizontally towards the entrance point as the single CTCs do. The cluster then encounters another pillar which is slightly lateral to the previous pillar and the process is repeated. Due to the small horizontal displacement between the pillars, the small clusters end up moving horizontally while the single CTCs only move vertically. At the bottom of the chip, the individual CTCs are collected directly below the entry point while the small CTC clusters are collected from an outlet lateral to the entry point. After stage 2 of cluster separation, single CTCs and other naturally found cells within the blood move onto the Labyrinth in order to separate the CTCs from the other naturally found cells in the blood sample.

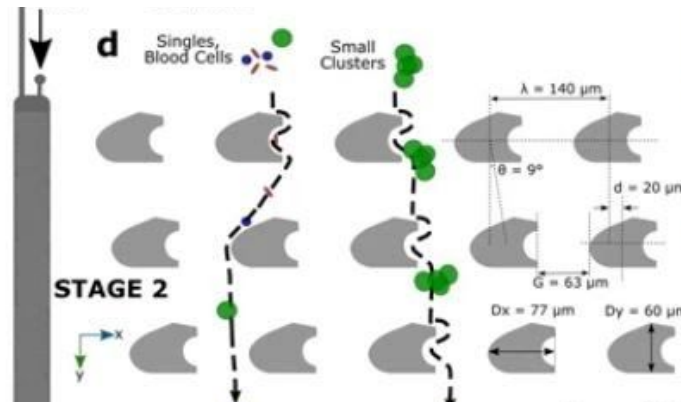


Figure A.2: Cartoon sketch of Stage 2 of the CTCC separator showing the DLD process. Adapted from Ref A2.

A.3 Requirement List

- Less than 2 hour testing time
- Testing for sepsis, CTCs, and CTCCs, and assessing leukemia and lymphoma
- \$1500 budget
- 2 month time limit

A.4 Sketches/Alternate Designs

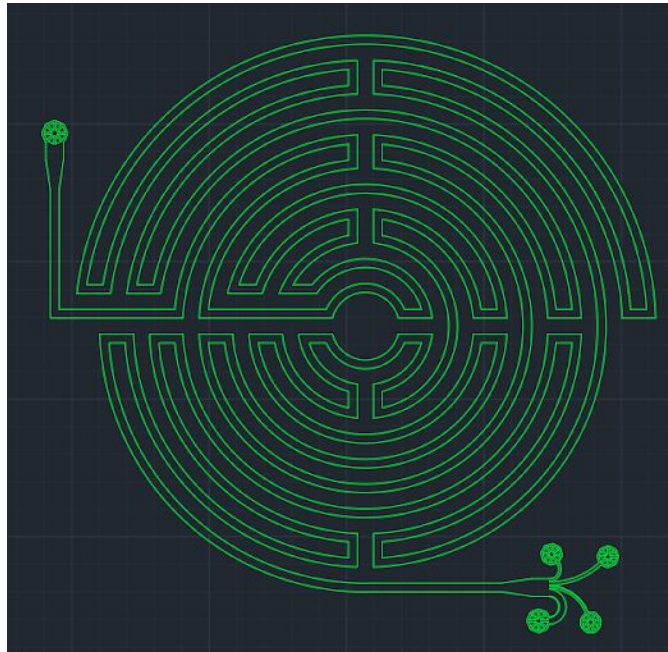


Figure A.3: The original AutoCAD for the Labyrinth section based on the respective reference literature.

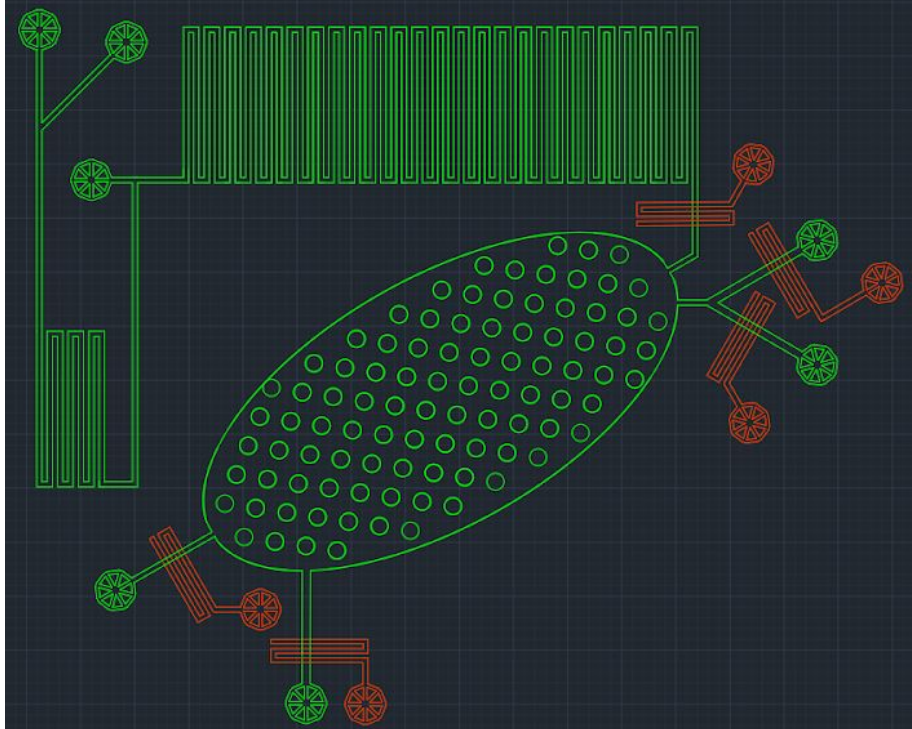


Figure A.4: The original AutoCAD for the later discarded CD64 antibody-based sepsis analyzer. Red layer symbolizes control layer. Green layer symbolizes flow layer.



Figure A.5: The original AutoCAD for the 2-phase CTCC separator based on the respective reference literature.

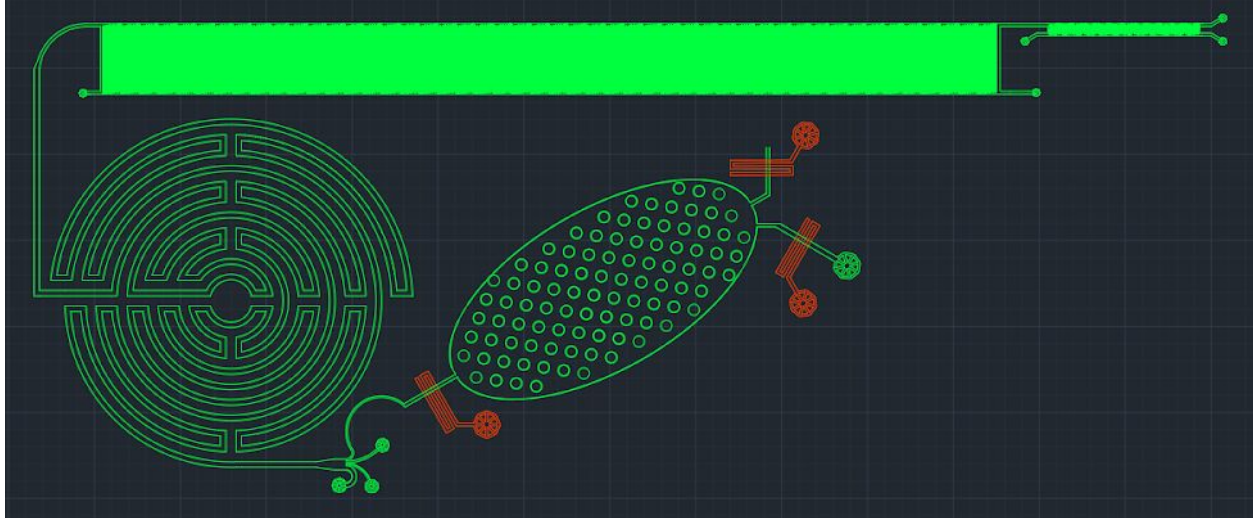


Figure A.6: First draft of the combined system with the 2-phase CTCC separator, Labyrinth design, and CD64 antibody-based sepsis analyzer.

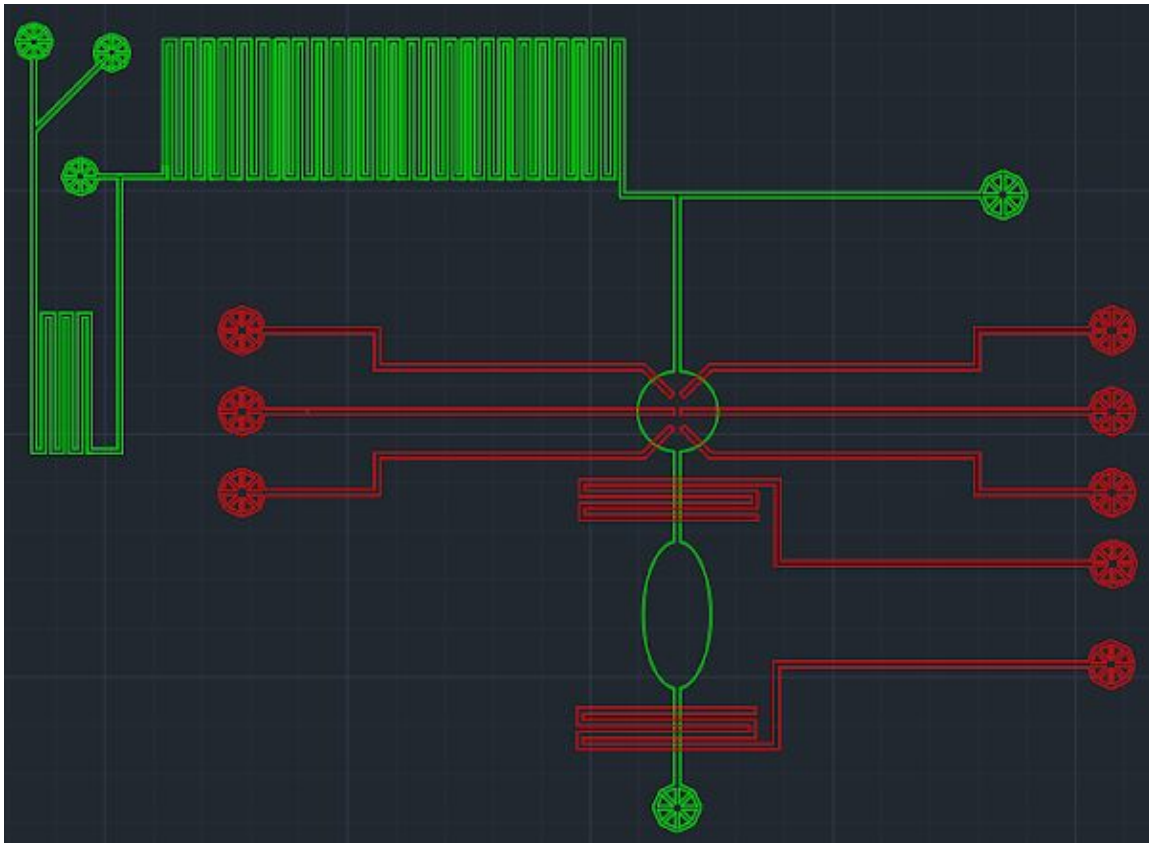


Figure A.7: New design for sepsis analysis based on fluorescent CD64 analysis using rotary mixer and lysing/quenching maze.

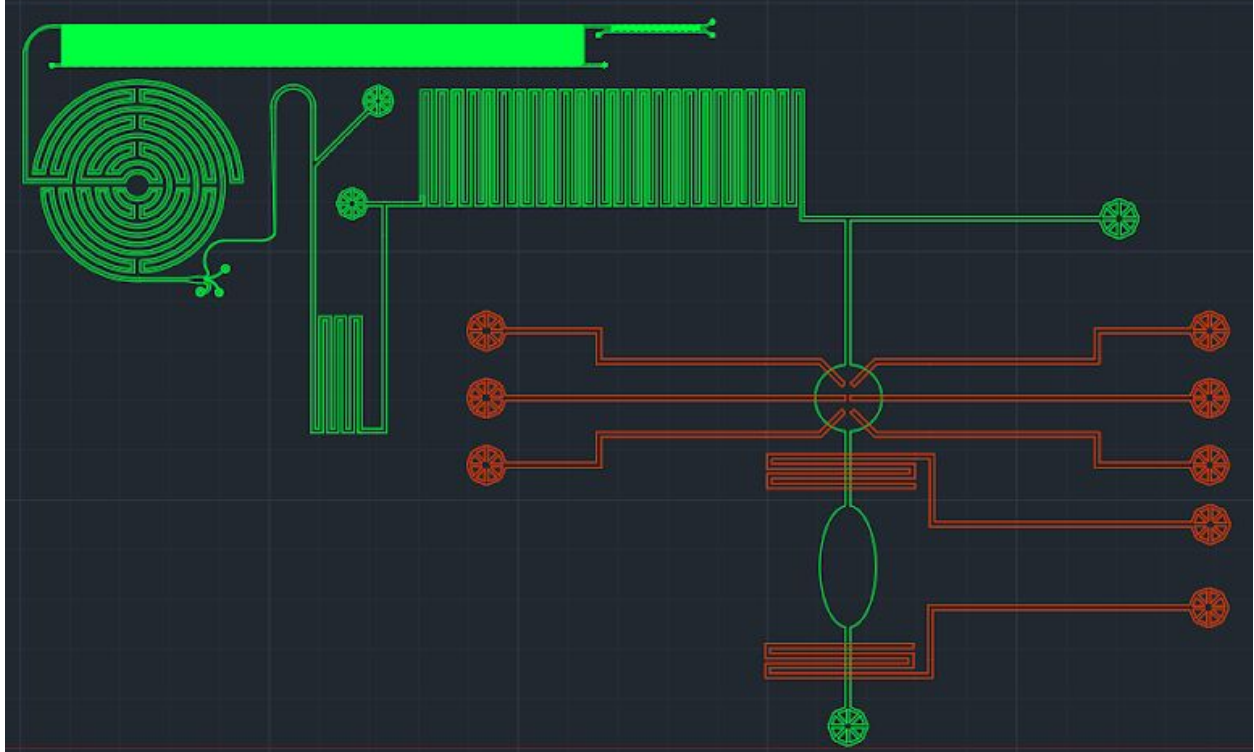


Figure A.8: Second draft of the combined system with the 2-phase CTCC separator, Labyrinth design, and new design for sepsis analysis based on fluorescent CD64 analysis using rotary mixer and lysing/quenching maze.

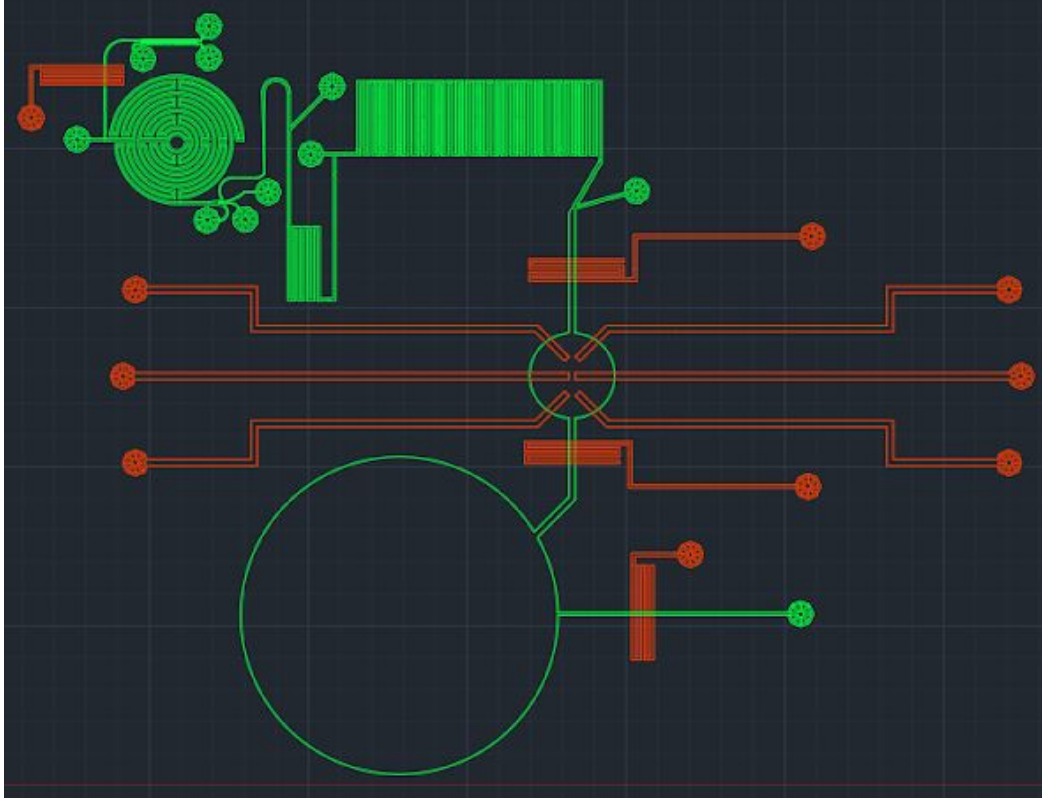


Figure A.9: Third draft of the combined system with the first phase of the CTCC separator, Labyrinth design, and sepsis analyzer based on fluorescent CD64 analysis using rotary mixer and lysing/quenching maze. Resized valves and large imaging chamber added.

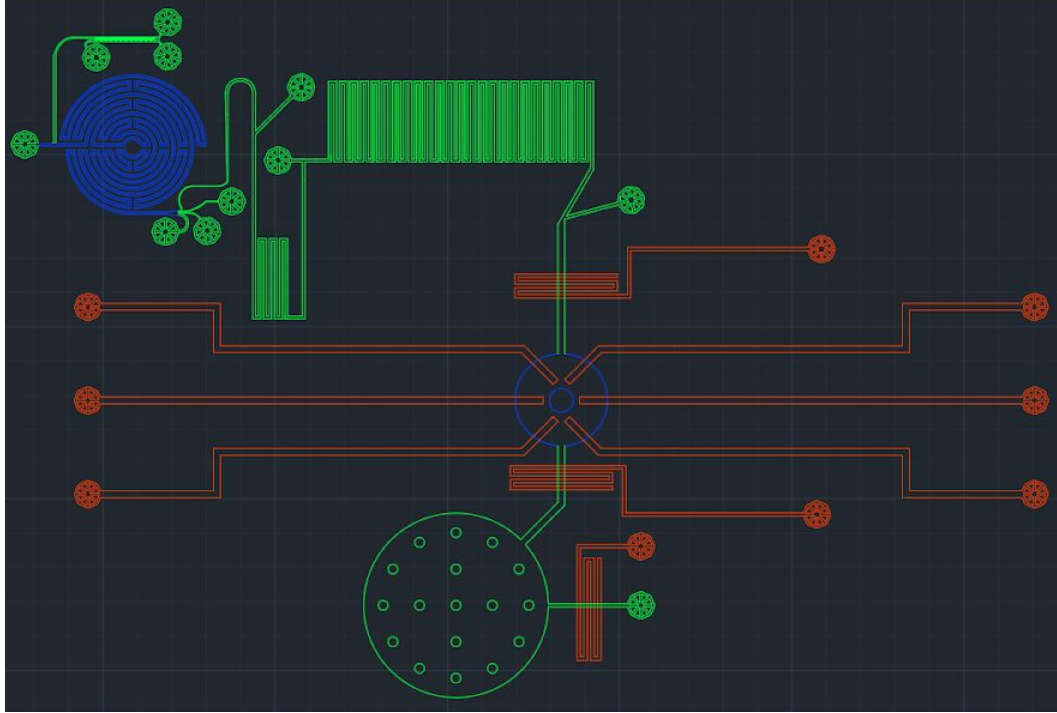


Figure A.10: Fourth and final draft of the combined system with the first phase of the CTCC separator, Labyrinth design, and sepsis analyzer based on fluorescent CD64 analysis using rotary mixer and lysing/quenching maze. Mixing and imaging chambers resized and pillars added to increase structural integrity. Color added to differentiate layers.

A.5 Decision Rationale

As seen above, we went through several different versions of some of the components, as well as several versions of the overall design. We started with AutoCAD designs largely based on the reference figures, but quickly adapted them based upon some aspects that needed to be changed. The main and largest change was from the CD64 antibody-based sepsis analyzer seen in **Figures A.4 and A.6** to the new device based on mRNA seen in **Figures A.7 through A.10**.

We decided to create our own device for sepsis assessment rather than utilizing designs from our literature review because these designs lacked important characteristics which we desired for our design. One design which we initially focused on, utilized antibodies to capture and enumerate CD64 expressing WBC's for sepsis diagnosis. The problems with this design, and other designs similar to it, is that they are overly complicated and take a significant amount of time to complete the test. The operating time is incredibly important for sepsis diagnosis because

the disease progresses rapidly, so the diagnosis must be very quick. When creating our sepsis diagnosis design, we focused on reducing the time of operation and complexity of our device in order to get quick results and allow facilitated integration with other components in our system.

The next few modifications to the design came from removing the second phase of the cluster separator, resizing the mixing and imaging chambers for sepsis analysis, resizing the valves, and adding a new layer. The removal of the second phase of the cluster separator was largely based around reducing the time, given that the original CTCC separation time was 7.53 hours, and removing phase 1 reduced that time by 6.49 hours. Additionally, the main point of the second phase, to remove small CTCCs, can be accomplished by the Labyrinth. This also rescues complexity of the design.

The resizing of the imaging and icing chambers was because we initially had the idea to have only one layer of WBC components for imaging, but we soon realized that this forced the imaging chamber to be too large. This is also why we added pillars to add structural integrity, since even the smaller size was still not stable and would likely be prone to collapse. We also resized all of the valves to a single size for simplicity and better accessibility. The blue layer was added because the larger height of the Labyrinth component and mixing chamber does not allow for them to be printed within the same layer as Flow or Control.

A.6 Calculations

Time version 1

①

$$1 \text{ mL} = 1000 \mu\text{L}$$

$$7.5 \text{ mL} = 7500 \mu\text{L}$$

* 16.6 mL/min flow rate

$$\frac{7500 \mu\text{L}}{16.6 \mu\text{L}/\text{min}} = 451.81 \text{ min}$$

$$= 7.53 \text{ hr}$$

②

$$7.5 \text{ mL} \quad 15 \text{ min (given)}$$

* 2 mL/min

③

Lyse - 6.2 $\mu\text{L}/\text{min}$
 Quench - 3.3 $\mu\text{L}/\text{min}$

10 μL (given)

Lyse time = 6.1 sec
 Quench time = 38.24 sec

1000 μL
 1 mL

$T_L = T_{L10} (100) = 600.1 \text{ sec} \approx 10 \text{ min}$
 $T_Q = T_{Q10} (100) = 3824 \text{ sec} \approx 1 \text{ hr}$

7.5 mL

$T_L = T_{L1} (7.5) = 4500.75 \text{ sec} \approx 1 \text{ hr } 15 \text{ min}$
 $T_Q = T_{Q1} (7.5) = \frac{428 \text{ min}}{28680 \text{ sec}} \approx 8 \text{ hr}$

Total Time (7.5 mL) = 7.53 hr + 0.25 hr + 1.25 hr + 8 hr $\approx 17 \text{ hr}$
 Way too long!!!

- ① CTCC 2-phase
- ② Labyrinth
- ③ Sepsis Analysis Machine

Figure A.11: First version of time test, calculated by design section. Time is too long, requiring design changes

Blood Components
 10mL blood - 5×10^5 RBC
 8×10^7 WBC
 $+ 3 \times 10^9$ platelet

 3.0805×10^9 particles

$$\text{WBC's } \sim 100 \times \frac{8 \times 10^7}{3.0805 \times 10^9} = 2.6 \%$$

$$2.6 \% \text{ of } 9.25 \text{ hr} = .24 \text{ hr} = 14 \text{ min}$$

Assume 10 min for
 imaging + 10 min mixing

$$= \text{34 min SAM}$$

Figure A.12: Blood component calculations, based on only WBCs needing to be analyzed for sepsis. Findings show significant time reduction for sepsis analyzer

Time Version 2
① Unchanged from V1
7.53 hr

② Unchanged from V1
0.25 hr

③ WBC only
14 min Lyse/Quench
10 min mix
10 min image
34 min

$$\begin{aligned} \text{Total} &= 7.53 \text{ hr} + 0.25 \text{ hr} + 0.57 \text{ hr} \\ &= 8.35 \text{ hr} \end{aligned}$$

still too long

① CTCC 2-phase

② Labyrinth

③ SAM WBC-only

Figure A.13: Second version of time test, calculated by design section and based on blood component calculations. Time is better, but still too long, requiring further design changes

CTCC Separator

Length Calculation - L

$$\begin{array}{l} \text{Total } L = 100,010.85 \text{ mm} \\ L_1 = 13800 \text{ mm} \\ L_2 = 81843.3 \text{ mm} \end{array}$$

$$L_1/L_T = \frac{13800}{100010.85} = 0.138 = 13.8\%$$

$$L_2/L_T = \frac{81843.3}{100010.85} = 0.818 = 81.8\%$$

Removing Stage 2 of CTCC Sep.
reduces time to 13.8%

$$0.138 \times 7.53 \text{ hr} = 1.04 \text{ hr}$$

Reduces time by 6.5 hr

Significant Reduction

Figure A.14: Time calculation for CTCC separator based on length. Removing Stage 2 appears to be a necessary time-saving measure eliminated by redundancy from the Labyrinth

Time Version 3

$$\begin{aligned} \textcircled{1} \quad L_1 &= 0.138 L_T \\ T_{L_1} &= 0.138 T_{LT} \quad , \quad T_{LT} = 7.53 \text{ hr} \\ T_{L_1} &= 0.138 (7.53) = \underline{1.04 \text{ hr}} \end{aligned}$$

$\textcircled{2}$ Unchanged from V1
15 min

$\textcircled{3}$ Unchanged from V2
34 min

$$\text{Total} = \begin{matrix} 1.04 & + & 0.25 & + & 0.57 \\ \text{hr} & & \text{hr} & & \text{hr} \end{matrix}$$

$$= 1.86 \text{ hr} \leftarrow 2 \text{ hr} \checkmark$$

$\textcircled{1}$ CTCC 1-phase

$\textcircled{2}$ Labyrinth

$\textcircled{3}$ SAM WBC-only

Figure A.15: Third version of time test, calculated by design section and based on CTCC length calculation. Time is within 2 hours, which meets our goal

Leukocytes = 12-15 μm
10 mL blood = 8×10^7 WBCs

$$A = \pi r^2 = \pi (15)^2 \quad \text{Allow for movement or buffer}$$
$$= \pi (18)^2 \quad \text{Area to fit 1 WBC}$$
$$= 1017.88 \mu\text{m}^2$$

$$8 \times 10^7 \times 1017.88 \times \frac{7.5 \mu\text{L}}{10 \mu\text{L}} = 6.1073 \times 10^{10} \mu\text{m}^2$$

Area
7.5 μmL
sample

$$6.1073 \times 10^{10} \mu\text{m}^2 = \pi r^2$$

$r = 1,394,27,4005 \mu\text{m}$
Radius of imaging chamber
needed for 1-layer imaging

1-layer \gg 235,000 μm
width of entire
Device

New Plan Needed

Figure A.16: Calculation of size of imaging chamber needed for 1-layer imaging. Size reduced to allow for 2-3 layers, reducing size needed

A.7 Academic Timeline for Microfluidic Liquid Biopsy for Cancer Prognosis

	Spring Quarter 2020
Week 1	Literature Review and Research
Week 2	Literature Review and Research
Week 3	Literature Review and Research
Week 4	Initial Idea Proposal and Design
Week 5	Initial AutoCAD Design and Additional Research
Week 6	Sepsis Assessment Research and Section Addition
Week 7	Secondary AutoCAD Design and Additional Research
Week 8	Final Design Creation and Restructuring
Week 9	Senior Design Presentation
Week 10	Final Thesis Completion

A.8 Literature Review

1) Sarioglu, A., Aceto, N., Kojic, N. *et al.* A microfluidic device for label-free, physical capture of circulating tumor cell clusters. *Nat Methods* 12, 685–691 (2015).

<https://doi.org/10.1038/nmeth.3404>

This study utilizes a “Cluster Chip” design to isolate circulating tumor cell clusters from unprocessed blood with a high capture efficiency for breast and prostate cancers. The design captured 99% of CTCCs that were composed of 4+ cells, 70% of 3 cell CTCCs, and 40% of 2 cell CTCCs. This chip flowed the whole blood sample at a rate of 2.5ml/h utilizing many different raised triangular pillars with integral separation points where the vertices of the triangles meet. This small space between the vertices allows normal blood cells and single circulating tumor cells through but holds CTCCs. Even if the CTCCs are oligoclonal, the

bifurcating edge of the triangular pillar provides a dynamic force balance utilizing cell-cell connecting forces to hold the CTCCs.

The cluster chip method outperforms membrane-based separation methods for CTCC separation. Pore based filtration tends to break up or lose CTCCs during wash steps. Therefore, utilizing the cluster chip methods results in a higher capture efficiency than membrane-based separation methods. In addition, this method outperforms antibody-based microfluidics for CTCC capture by 50-400%.

2) Aceto, N., Bardia, A., Miyamoto, D. T., Donaldson, M. C., Wittner, B. S., Spencer, J. A., Yu, M., Pely, A., Engstrom, A., Zhu, H., Brannigan, B. W., Kapur, R., Stott, S. L., Shioda, T., Ramaswamy, S., Ting, D. T., Lin, C. P., Toner, M., Haber, D. A., & Maheswaran, S. (2014). Circulating tumor cell clusters are oligoclonal precursors of breast cancer metastasis. *Cell*, 158(5), 1110–1122. <https://doi.org/10.1016/j.cell.2014.07.013>Metastasis

This article describes the CTCC formation process in detail with a focus on intracellular connection. The study utilizes mouse models with tagged mammary tumors to demonstrate that CTCCs form from oligoclonal tumor cell groupings rather than intravascular aggregation. The intracellular CTCC connection relies on a protein known as plakoglobin and the abrogation of this protein prevents CTCC formation.

This study demonstrates that CTCCs have a 23-50 fold increased metastatic potential, that CTCCs represent 2-5% of total CTCs. The study also shows that CTCCs have better vascular integrity and longevity, surviving roughly three times longer than CTCs when in circulation.

3) Au, S.H., Edd, J., Stoddard, A.E. *et al.* Microfluidic Isolation of Circulating Tumor Cell Clusters by Size and Asymmetry. *Sci Rep* 7, 2433 (2017). <https://doi.org/10.1038/s41598-017-01150-3>

This study utilizes a two-stage continuous microfluid chip to separate CTCCs from a whole blood sample using deterministic lateral displacement capitalizing on size and asymmetry. The first stage of the chip utilizes rows of slightly offset pillars which allow small clusters and cells to weave through the pillars while forcing large clusters towards the right side of the chip through deterministic lateral displacement where they can be captured. The second stage of the chip uses rows of slightly offset asymmetric pillars with a cleft on their right side to separate smaller CTCCs from single CTCs and blood cells. This second stage utilizes a low ceiling to force small CTCCs to flatten and rotate through the pillars due to their asymmetry. This forces the small CTCCs to be unable to weave through the pillars and instead move horizontally through deterministic lateral displacement to the right side where they are collected. The single cells and whole blood are able to weave around the pillars and become separated from small CTCCs.

Large CTCCs were designated as having 8+ cells per cluster, and small CTCCs were designated as having 2-8 cells per cluster. This pillar microfluidic design had a flow rate of .5ml/h and resulted in a 98.7% capture efficiency for large CTCCs and 65.5% capture efficiency for small CTCCs. This study had similar, but slightly lower, whole blood CTCC capture efficiencies when compared to the Cluster Chip design (Source 1).

4) Chou, W.-P., Chiu, T.-K., & Chao, A.-C. (2018). Optically-induced-dielectrophoresis (ODEP)-based cell manipulation in a microfluidic system for high-purity isolation of integral circulating tumor cell (CTC) clusters based on their size characteristics. *Sensor and Actuators B: Chemical*, 258, 1161–1173. Retrieved from https://www.sciencedirect.com/science/article/abs/pii/S0925400517323298?casa_token=DEUa4lxqwb8AAAAA:D1_4zxuRwc3peWX9AL1Jf9rIo5OCzu0A-ZquYeF0_MB-MUkTTwzN3XH2yZiHVmFQu0lwW3utKg

This article utilizes optically induced dielectrophoresis (ODEP) based cell manipulation to separate CTCs and CTCCs based on their size characteristics. The chip utilizes an AC current to create an electric field which becomes dynamic based on how the light source hits the

photoconductive layer. This dynamic electric field is utilized to separate cells and microparticles based on the size of relative cells, clusters, and particles. This ODEP separation process involves two steps. In the first step, a dynamic square light image array separates CTCCs and in the second step, another ODEP based cell manipulation to refine the purity of the harvested CTCCs. This separation process had a cell purity rate of 91.5% and a recovery rate of 70.5%.

This optically induced dielectrophoresis separation mechanism had a significantly lower CTCC separation efficiency than simple size and shape based microfluidic separation mechanisms analyzed previously such as the cluster chip and the pillar chip.

5) Xu, L., Mao, X., Imrali, A., Syed, F., Mutsvangwa, K., Berney, D., Cathcart, P., Hines, J., Shamash, J., & Lu, Y. J. (2015). Optimization and Evaluation of a Novel Size Based Circulating Tumor Cell Isolation System. *PloS one*, 10(9), e0138032.
<https://doi.org/10.1371/journal.pone.0138032>

This article performs a review of the Parotix CTC and CTCC separation system. This system utilizes extracellular ligands found on CTCs and CTCCs to separate them from whole blood samples. Problems with the study include the inconsistency of available ligands on CTCs for binding. The study utilizes an immunofluorescence based system for quantification of captured cells and achieved a separation of roughly 60% depending on cell type and buffer use.

This article compared the Parotix separation system to the Cell Search and IsoFlux systems and achieved a similar separation efficiency to them. In addition, this article had a focus on CTC capture however it also captured CTCCs as well. The separation efficiencies of the optimized Partotix system are roughly 30% lower than the Cluster Chip and Pillar based CTCC separation mechanisms.

6) Mario Giuliano, Anum Shaikh, Hin Ching Lo, Grazia Arpino, Sabino De Placido, Xiang H. Zhang, Massimo Cristofanilli, Rachel Schiff and Meghana V. Trivedi (2018). Perspective on Circulating Tumor Cell Clusters: Why It Takes a Village to Metastasize. *Cancer Res* February 15 2018 (78) (4) 845-852; DOI: 10.1158/0008-5472.CAN-17-2748

This article includes a thorough description of the mechanisms involved in CTCC metastasis and highlights the importance of research in this area. CTCCs not only have a roughly 40-50 times higher chance of resulting in successful metastasis but they also may result in communication between tumor sites and explain how certain cancers can survive extensive treatment pressures. In addition, the clusters have a higher rate of survival within circulation, which is likely due to adhesive cooperation of the cells within the cluster to counteract shear forces, environmental and oxidative stress, and immune assaults.

This article also highlights the benefits of using microfluidic devices for CTCC separation and which microfluidic designs are most effective for cluster separation. Microfluidic devices are effective for cluster separation because they are able to process whole blood without the need for RBC removal and because they can separate CTCCs without killing them. The article states that spiral systems, the cluster-chip platform, and deterministic lateral displacement are the most effective microfluidic designs for cluster separation.

7) Vasudha Murlidhar, Rishindra M. Reddy, Shamileh Fouladdel, Lili Zhao, Martin K. Ishikawa, Svetlana Grabauskiene, Zhuo Zhang, Jules Lin, Andrew C. Chang, Philip Carrott, William R. Lynch, Mark B. Orringer, Chandan Kumar-Sinha, Nallasivam Palanisamy, David G. Beer, Max S. Wicha, Nithya Ramnath, Ebrahim Azizi and Sunitha Nagrath (2017). Poor Prognosis Indicated by Venous Circulating Tumor Cell Clusters in Early-Stage Lung Cancers *Cancer Res September 15 2017 (77) (18) 5194-5206*; DOI: 10.1158/0008-5472.CAN-16-2072

This article assesses the efficacy of prognosis based on the detection of circulating tumor cells and their clusters from whole blood in different locations within the body. The blood was obtained during tumor removal surgeries from pulmonary veins and peripheral veins. The study found that there was a higher concentration of CTCs and CTCCs in pulmonary veins than peripheral veins and this is alarming due to the potential mobility of the location.

In addition this article found that 50% of the tested patients had circulating tumor cell clusters in their blood. This consistency is much higher than estimates based on the rarity of these clusters. This high consistency is also very problematic due to the significantly higher

metastatic potential associated with clusters. The study also found that the presence of circulating tumor cell clusters was associated with poor prognosis. This is likely due to the high metastatic potential associated with these cell clusters.

8) Yoon, Y., Lee, J., Ra, M., Gwon, H., & Lee, S. (2019). Continuous Separation of Circulating Tumor Cells from Whole Blood Using a Slanted Weir Microfluidic Device. *MDPI*, *11*(2). doi: <https://doi.org/10.3390/cancers11020200>

Design Specifications:

- 4.5×4.5 cm² surface oxidized silicon chip.
- Main Channel is 500µm
- Double-layer photolithography was used to pattern the slanted weir integrated microfluidic channel
- The first layer was spin-coated with a SU-8 2050 (Microchem, Westborough, MA, USA) photoresist, which was 23 µm thick, and the weir structure was patterned.
- The second layer, which defines the weir gap, was spin-coated with the SU-8 2007 (Microchem) photoresist, which was 7 µm thick.

Efficiency:

- Dependent on Weir angle, multiple were tested.
- The weir angles that produced $\Delta P_x/\Delta P_y > 1$ (0.5° and 0.8°) resulted in very high separation efficiencies, showing values of ~95% efficiency.

Flow Rate:

- ΔP_y should be 50 PA, therefore, ΔP_x should be slightly higher (50-60PA)
- The sample-to-buffer flow rate ratio must be 1:4 or with a higher portion of the buffer flow rate.
- The total flow rate was set at 2.5 mL/h for the 0.8° weir and at 3.8 mL/h for the 0.5° weir, which produced a ΔP_y of 50 Pa

9) Zhou, J., Kulasinghe, A., Bogseth, A. *et al.* Isolation of circulating tumor cells in non-small-cell-lung-cancer patients using a multi-flow microfluidic channel. *Microsyst Nanoeng* 5, 8 (2019). <https://doi.org/10.1038/s41378-019-0045-6>

Specifications:

- Replicated straight channels (150 μm wide, 50 μm high, and 20 mm long) in PDMS were bonded to 1" \times 3" glass slides
- Microchannels were fabricated via standard soft photolithography.

Other inertial migration testing also utilized this channel sizing

(<https://www.ncbi.nlm.nih.gov/pmc/articles/PMC6356955/>)

Efficiency:

- For cell line H460, the recovery rate is more than 93%

Flow Rate:

- The flow rate ratio is defined as the sample flow rate (Q_s) over the buffer flow rate (Q_b). The total flow rate ($Q_t = Q_s + Q_b$) was fixed at 300 $\mu\text{L}/\text{min}$, equivalent to $Re = 50$.

10) Mustjoki S, Sidenius N, Sier CF, et al. Soluble urokinase receptor levels correlate with number of circulating tumor cells in acute myeloid leukemia and decrease rapidly during chemotherapy. *Cancer Res.* 2000;60(24):7126-7132.

This article focuses on plasminogen activation and its role in metastasis specifically for acute myeloid leukemia. The study focuses on urokinase(uPA) and its receptor (uPAR) and shows that they have a significant role in the cell migration and tumor cell invasion aspects of metastasis. Data has shown that the upregulation of uPAR correlates with a poor response to chemotherapy and that for leukemia specifically, high levels of plasma soluble uPAR (suPAR) also correlates with a poor response to chemotherapy.

This study measured levels of uPAR in cells, plasma, and urine in patients with acute leukemia throughout a 56-day time frame. The results were that, as levels of CTCs decreased with chemotherapy, levels of suPAR decreased as well. However, bone marrow aspirations of patients with acute leukemia demonstrated excessive levels of suPAR. These results suggest that CTCs secrete excessive amounts of suPAR likely as a means to escape the danger of circulation and migrate into other parts of the body creating secondary tumor sites.

11) Kulasinghe, A., Zhou, J., Kenny, L., Papautsky, I., & Punyadeera, C. (2019). Capture of Circulating Tumour Cell Clusters Using Straight Microfluidic Chips. *Cancers*, 11(1), 89. <https://doi.org/10.3390/cancers11010089>

In this study, the authors investigated the presence of CTCs and circulating tumor microemboli (CTMs) in head and neck cancers using a novel straight microfluidic chip technology that exploits size-based differences between CTCs and haematopoietic cells. The device has a channel width of 150 μm and height of 50 μm , with two inputs and two outputs. Buffer (PBS) is introduced at the inner inlet and sample at the outer inlet, which forms two sample flows sandwiching a buffer flow in the middle of the microchannel. Cells migrate laterally away from the sample streams into the clean buffer stream due to inertial forces. The channel length can be precisely controlled to select larger CTCs and clusters, separating them from WBCs, because inertial migration is strongly dependent on size. CTCs and clusters are collected in the inner outlet and all other waste cells exit the channel through the outer outlet. Operating at a flow rate of 100 and 200 $\mu\text{L}/\text{min}$ for the sample and PBS solution respectively, the device was tested with several spike-in and recovery experiments using three HNC cell lines. The percentage recovery for cell counts between 50–500 cells ranged from 70–96%, and 40–80% for spike-in experiments of 10 cells. The researchers also tested the device on head and neck cancer (HNC) patient blood samples, and found that single CTCs and CTC clusters were present at all stages of the disease.

This device overcomes the limitations of current CTC enrichment technologies that use surface marker expression (positive selection), or the removal of non-cancer cells (negative

selection) to enrich cancer cells. These positive and negative selection methods are poor in discriminating between individual CTCs and CTC clusters. However, a limitation of this microfluidic chip is that small CTCs, which have a comparable size to WBCs, are unlikely to be captured using size based exclusion technologies.

12) Lin et al. (2017). High-Throughput Microfluidic Labyrinth for the Label-free Isolation of Circulating Tumor Cells. *Cell Systems* 5, 295–304 September 27, 2017
<http://dx.doi.org/10.1016/j.cels.2017.08.012>

The authors of this study designed a device inspired by the Labyrinth in Greek mythology, which was an elaborate structure with numerous turns and corners built to hold the Minotaur. The “Labyrinth” is a label-free microfluidic device that isolates circulating tumor cells (CTCs) using the combination of long loops and sharp corners to focus both CTCs and white blood cells (WBCs). The total channel length of the Labyrinth is 637 mm, the channel is 500 μm in width and 100 μm in height, and it consists of 11 loops and 56 corners. The loops, which have a small curvature ratio, provide enough length of channel to achieve total focusing of cells and to have the proper curvature for the separation of CTCs and blood cells. The 56 sharp right-angle corners, which have high curvature ratio, further enhance the focusing of smaller cells. The channel expands from a width of 500 μm to 1000 μm before diverting into four separate outlets to collect WBCs, CTCs, RBCs and other blood components. The percent recovery in outlet 2 during one of the control experiments was 91% for WBCs, 92% for PANC-1 cells, 90% for H1650 cells, and 91% for MCF-7 cells to list a few.

The reason the authors wanted to develop a label-free isolation method is because many microfluidic devices rely on positive or negative selection to isolate CTCs, such as the immune-affinity capture method that utilizes antibodies to target molecules, such as the epithelial cell adhesion molecule (EpCAM), which are expressed exclusively on tumor cells. The drawback with these methods however, is that not all CTCs express EpCAM, and downstream single cell-analysis of captured CTCs can be challenging due to complex protocols that may interfere with RNA stability during the release step of CTCs from devices.

13) Wan, S., Kim, T.H., Smith, K.J. et al. New Labyrinth Microfluidic Device Detects Circulating Tumor Cells Expressing Cancer Stem Cell Marker and Circulating Tumor Microemboli in Hepatocellular Carcinoma. *Sci Rep* 9, 18575 (2019).
<https://doi.org/10.1038/s41598-019-54960-y>

The authors of this study developed and optimized a novel Labyrinth microfluidic device to efficiently isolate CTCs from peripheral blood of Hepatocellular Carcinoma (HCC) patients. They made modifications to the original Labyrinth and increased the height of the channel to 110 μm . This modification increased the Dean force effect, allowing the cells to equilibrate at similar focusing positions at lower flow velocities, which reduced the overall shear stress acting on the CTCs during separation. The Labyrinth device has an inlet to inject the sample, and four outlets. Outlet 1 collects WBCs, outlet 2 collects CTCs, and outlets 3 and 4 were included to reduce the sample fluid volume after cell separation and collection. Spike-in experiments to determine the recovery rate of CTCs in outlet 2, at the determined optimal flow rate of 2000 $\mu\text{L}/\text{min}$, revealed a recovery rate of 91.17% and 95.69% for Hep 3B and Hep G2 cells respectively after considering only the cells with a size above the cut-off cell diameter entering the outlet. The WBC depletion rate at this optimal flow rate was determined to be $97.66 \pm 0.53\%$. After optimizing the flow rate of the Labyrinth with spike-in experiments, the researchers tested the device with peripheral blood from HCC patients, and identified CTCs in 88.1% of the patients over different tumor stages. Interestingly, they also found that 55% of the patients had the presence of circulating tumor microemboli (CTM), sometimes referred to as circulating tumor cell clusters (CTCCs).

14) Kamyabi, N., Huang, J., Lee, J., et al. A microfluidic device for label-free isolation of tumor cell clusters from unprocessed blood samples. *Biomicrofluidics* 13, 044111 (2019)
<https://doi.org/10.1063/1.5111888>

In this study, the authors wanted to address some of the drawbacks of other devices designed to isolate CTC clusters. Microfilters have been used to capture clusters, because

clusters are significantly larger than single cells and can be arrested at the pores of the filter. The major drawback of this method is that you are prone to lose some of the clusters due to their deformability and subsequent transit through the pores. Another device, called the Cluster-Chip, contains a parallelized array of equilateral triangle shaped pillars. Clusters are wedged within a three-pillar unit, arrested due to a dynamic force balance between cell-cell adhesion strength, fluid drag forces, wall friction, and reactionary forces from the pillars. The potential drawback of this device is the possibility of cluster damage and inefficient capture because of the fact that the triangular pillars have sharp edges and the clusters interact with multiple three-pillar units.

The authors developed a new microfluidic device for isolating CTC clusters (“Microfluidic Isolation of CTC Clusters” or MICC platform) from unprocessed blood samples. The MICC platform is equipped with approximately 10,000 trap chambers that isolate tumor cell clusters based on their large sizes and dynamic force against a pillar obstacle in the trap chamber, similar to the Cluster-Chip. One of the factors that makes CTC cluster separation so difficult is that the shear forces in typical microfluidic devices are strong enough to separate the clustered CTCs. In the trap chamber of the MICC platform, the dynamic forces holding a cluster together are stronger than shear forces, so cluster separation is not an issue. Under optimal flow conditions and using blood samples spiked with different concentrations of clusters, the MICC platform performed with a capture efficiency of 66%–87% and release efficiency of 76%–90%.

15) Gou, Y., Zhang, S., Sun, C., Wang, P., You, Z., Yalikun, Y., . . . Ren, D. (2019). Sheathless Inertial Focusing Chip Combining a Spiral Channel with Periodic Expansion Structures for Efficient and Stable Particle Sorting. *Analytical Chemistry*, 92(2), 1833-1841.
doi:10.1021/acs.analchem

In this study, the authors improve upon the typical spiral channel microfluidic device by incorporating periodic expansion structures for the sheathless separation of particles with different sizes. The inertial lift force, which these microfluidic devices rely on to separate particles, is difficult to quantitatively analyze because of the uncertainties of its magnitude and direction. This means that the equilibrium position of the particles varies along the migration

process, thus inducing the instabilities of particle separation. In the spiral channel microfluidic device with periodic expansion structures, a stable vortex-induced lift force arises from the periodic expansion. The stable vortex-induced lift force along with the Dean drag force significantly enhance the focusing process, with experimental results showing that over 99% of target particles could be isolated with the high target sample purity of 86.12%.

16) Icardi, M., Erickson, Y., Kilborn, S., Stewart, B., Grief, B., & Scharnweber, G. (2009). CD64 index provides simple and predictive testing for detection and monitoring of sepsis and bacterial infection in hospital patients. *Journal of clinical microbiology*, 47(12), 3914–3919. <https://doi.org/10.1128/JCM.00628-09>

In this article, the authors conduct a study to confirm and extend the previous literature that provides evidence that granulocyte CD64 expression is predictive of sepsis and bacterial infection. They measured CD64 expression by granulocytes of 113 patient blood samples (4 were determined ineligible) using a Leuko64 kit (Trillium Diagnostics, ME) and a BD FACSCalibur running Quanticalc software (Verity Software House, ME). 24 blood samples from healthy individuals and 20 blood samples from patients who had undergone uncomplicated surgeries were used for controls. In each blood sample, lymphocytes were used as an internal negative control and monocytes as an internal positive control. After performing fluorescence-activated cell sorting (FACS), they calculated the CD64 index using the ratio of the mean fluorescent intensity of the cell populations (lymphocytes and monocytes) to that of the beads. In order for the internal controls to be considered valid, the lymphocytes should have a CD64 index of <1 and monocytes an index of >3 . After obtaining the CD64 indices of the blood samples and performing blood cultures, the researchers categorized the patients into four groups: no infection, clinical infection, culture-proven infection, and blood culture-proven infection. After performing statistical analysis and constructing receiver operating characteristic (ROC) curves for the CD64 index and WBC counts, the point of maximum test efficiency, sensitivity, specificity, likelihood ratios, and positive and negative predictive values were calculated (point of maximal efficiency = 1.19 (P value = 0.000019), sensitivity = 94.6%, specificity = 88.7%,

positive likelihood ratio = 8.36, negative likelihood ratio = 0.06, positive predictive value = 89.8%, negative predictive value = 94%). Comparing the CD64 indices to the blood culture results, it was determined that an index >1.19 detected all of the culture-positive patients and an index of ≤ 1.19 was 100% predictive of a “no-growth” blood culture.

The total turnaround time for this test is approximately 45 min, which is a huge improvement compared to the turnaround time of the gold standard for diagnosing sepsis, blood culture. It takes up to two days to obtain results from blood culture, and sepsis patients can experience severe complications within that time frame. This study validates our reason and motivation for selecting CD64 as a neutrophil biomarker in the diagnosis of sepsis associated with leukemia. We expect our microfluidic device to be more user friendly than FACS systems, and as a result will be able to be used by medical staff to constantly and consistently monitor patients suspected of having sepsis.

17) Yin, W. P., Li, J. B., Zheng, X. F., An, L., Shao, H., & Li, C. S. (2020). Effect of neutrophil CD64 for diagnosing sepsis in emergency department. *World journal of emergency medicine*, 11(2), 79–86. <https://doi.org/10.5847/wjem.j.1920-8642.2020.02.003>

The authors of this study investigated the diagnostic and prognostic value of neutrophil CD64 (nCD64) as a novel biomarker in sepsis patients, and compared it to other indicators of bacterial infection such as elevated levels of C-reactive protein (CRP), procalcitonin (PCT), and white blood cells (WBC). WBC count, PCT levels, and CRP levels were measured from 151 adult patients diagnosed with sepsis and 20 healthy controls. Samples of blood, urine, sputum, or bronchoalveolar lavage fluid were collected to perform bacteriological culture and confirm bacterial infection. Individual Sequential Organ Failure Assessment (SOFA) scores were calculated and patients were followed up for up to 28 days. nCD64 levels were determined by flow cytometry using residual blood from routine blood samples. After performing statistical analysis, it was determined that nCD64 expression was higher in the sepsis group with confirmed infection than in the control group. The receiver operating characteristic (ROC) curve of nCD64 was higher than those of SOFA score, CRP, PCT, and WBC for diagnosing infection. However,

the area under the curve (AUC) of nCD64 was slightly lower than the AUC of the SOFA score, which means that the SOFA score is better for predicting 28-day mortality in sepsis. That is why the authors concluded that combining both parameters, nCD64 expression and the SOFA score, was the best approach to diagnose sepsis early and improve patient outcomes.

This study also validates our reason and motivation for selecting CD64 as a neutrophil biomarker in the diagnosis of sepsis associated with leukemia, as it has been shown to outperform CRP, PCT, and WBC levels as indicators of sepsis. Even though the SOFA score was slightly better at predicting 28-day mortality in sepsis patients, the expression of nCD64 is in our opinion, the fastest and easiest parameter to measure in diagnosing sepsis because a SOFA score is merely a mortality prediction score that is based on the degree of dysfunction of six organ systems.

18) Marwaha, R. K., Kulkarni, K. P., Bansal, D., & Trehan, A. (2010). Pattern of Mortality in Childhood Acute Lymphoblastic Leukemia. *Journal of Pediatric Hematology/Oncology*, 32(5), 366-369. doi:10.1097/mpb.0b013e3181e0d036

In this study, the authors performed a retrospective analysis of 532 patient case records of children with acute lymphoblastic leukemia (ALL) in the period between January 1990 and December 2006. After analyzing the case records, it was determined that sepsis (53.3%) and bleeding (15.7%) were the most common causes of mortality in the 128 deaths that were recorded (24% death rate). When you contrast this death rate to the 2.6% death rate reported from an analysis of the causes of death, other than resistant disease or relapse, in 875 children with ALL treated on 3 different Dutch Childhood Oncology Group ALL protocols, the difference in death rates is astonishing. Survival rates in childhood ALL in developing countries with limited resources are inferior because of infection-related toxic deaths, a higher incidence of relapse, default of therapy, and loss to follow-up.

The main demographic we want our device to serve is children in developing countries, because as noted above, survival rates in childhood ALL in developing countries is lower than in developed countries because of the lack of resources. Our device will be readily available to

these countries because it will be easy and cheap to manufacture, as well as user friendly, eliminating the need for highly trained staff to perform other diagnostic tests such as flow cytometry or FACS to observe neutrophil CD64 expression. Additionally, our device integrates CTC and CTC cluster capture to provide additional diagnostic and prognostic information about the patient's cancer status.

19) Sin, A., Murthy, S. K., Revzin, A., Tompkins, R. G., & Toner, M. (2005). Enrichment using antibody-coated microfluidic chambers in shear flow: Model mixtures of human lymphocytes. *Biotechnology and Bioengineering*, 91(7), 816-826. doi:10.1002/bit.20556

The authors of this study were able to demonstrate the possibility of using dynamic cell attachment to antibody-coated microfluidic chambers in shear flow to enrich mixtures of MOLT-3 and Raji cells, both human lymphocyte cell lines. MOLT-3 cells are human immature T-lymphoblasts that express CD5 but not CD19, and Raji cells are human mature B-lymphocytes that express CD19 but not CD5. After incubating the cells and diluting them to a concentration of approximately 1×10^6 cells/mL, cell mixtures containing both cell lines were created. Shear stresses ranging between 0.75 and 1.0 dyn/cm² provided most efficient capture of cells based on affinity to antibody coated surfaces while reducing or eliminating undesired binding by the cell of interest. They were also able to verify that the dynamic cell adhesion of Raji and MOLT-3 follows a pseudo-first order kinetic model. They were able to obtain 100% pure MOLT-3 cells with an anti-CD19 coated device with approximately 2.6 min residence time, and around 75% Raji cells with an anti-CD5 coated device with approximately 3 min residence time. For both experimental tests, an almost 50-50 heterogenous cell mixture of MOLT-3 and Raji cells was used.

Other techniques currently used to isolate phenotypically-pure cell populations from heterogeneous cell mixtures include fluorescent activated cell sorting (FACS) and magnetic activated cell sorting (MACS). However, the drawback of these techniques is that they require pre-incubation with antibodies, which extends the processing time to at least 15-60 min. Our CD64+ neutrophil test is essentially doing the same as the device in this study, except that we are

enriching CD64+ neutrophils using an anti-CD64 coated microfluidic device in shear flow. This study demonstrates that under correct shear stresses, our device is very feasible and realistic.

20) Jackson, J. M., Taylor, J. B., Witek, M. A., Hunsucker, S. A., Waugh, J. P., Fedoriw, Y., Shea, T. C., Soper, S. A., & Armistead, P. M. (2016). Microfluidics for the detection of minimal residual disease in acute myeloid leukemia patients using circulating leukemic cells selected from blood. *The Analyst*, 141(2), 640–651. <https://doi.org/10.1039/c5an01836f>

In this study, the authors developed a microfluidic assay that was able to isolate and phenotypically identify leukemic cells circulating in a patient's peripheral blood. They performed a pilot clinical study where acute myeloid leukemia (AML) patients recovering from stem cell transplant (SCT) therapy were tracked by isolating CD33, CD34, and CD117 expressing circulating leukemic cells (CLCs) using three sinusoidal microfluidic devices arranged in a parallel configuration. Each device contains ≥ 50 parallel microchannels with a sinusoidal architecture and mAbs covalently attached to the surface of the channels. They were able to detect minimal residual disease (MRD) 28 days following SCT and the onset of relapse at day 57, which is a lot better than detection using PCR. PCR from a bone marrow biopsy did not detect MRD until day 85 of the same patient tested with the microfluidic assay.

While our project doesn't necessarily focus on CLCs in AML patients, this concept is something that future students should consider integrating into our device, maybe even replacing the CTC devices.

21) Tan, J., Ding, Z., Hood, M., & Li, W. (2019). Simulation of circulating tumor cell transport and adhesion in cell suspensions in microfluidic devices. *Biomicrofluidics*, 13(064105). doi: 10.1063/1.5129787

This paper focuses more on the modeling of CTC transport and adhesion than a new way to separate them, but it allows for the principles within to be applicable to both active and passive separation mechanisms. It also specifically mentions shifted post (columnar) passive separation designs, noting that the majority of cells only follow streamlines at low

concentrations. At standard concentrations, the collisions between red blood cells and CTCs or CTCs amongst each other cause a difference in trajectory from the expected streamline. This hampers the ability to create an accurate streamline-based model of cell trajectory for accurate sized-based filtration. This difference in trajectory increased with column size and cell concentration.

Simulation is also difficult due to the cell deformation affecting the flow and vice versa, in addition to the vast number of cells that need to be modeled to get an accurate concentration. This was solved using the lattice Boltzmann equation, immersed boundary method, and a coarse-grained molecular dynamics method to create an accurate computerized computational simulation model. Adhesion of the CTCs was also tested, finding “2562 [out of 2562] surface nodes can capture the cell deformation with a reasonable accuracy”.

“Based on the actuation mechanism, these microfluidic devices can be grouped into two categories: active ones and passive ones. Active microfluidic devices used external assistance such as magnetic field, electric field, optical forces, and acoustic fields to enrich CTCs. Among these methods, they either require sophisticated cell preparations, complex microfluidic designs, or external fields. On the other hand, passive devices utilize the hydrodynamics and physical properties of CTCs such as size, deformability, and specific binding between receptors expressed on cell membrane and ligands coated on microfluidic surfaces to separate CTCs from other cells.”

22) Chen, J., Liu, C.-Y., Wang, X., Sweet, E., Liu, N., Gong, X., & Lin, L. (2020). 3D printed microfluidic devices for circulating tumor cells (CTCs) isolation. *Biosensors and Bioelectronics*, 150(111900). doi: 10.1016/j.bios.2019.111900

This paper discusses the best way to 3D print a microfluidic device to capture CTCs from blood. These devices combined mechanical separation techniques with anti-EpCAM antibodies for capture and isolation. The paper also discusses the optimal flow rate (1 mL/h) and optimal channel length (2 cm) for these different designs. These designs were tested with breast, colon, and prostate cancer, all EpCAM positive, reaching a capture efficiency of around 90%. In

summary, this paper shows that 3D printed microfluidic devices can be just as effective as those created from other methods, as well as the details of how best to 3D print a microfluidic device.

- 3D printing technology was used to fabricate a microfluidic device that can increase inner surface area and manipulate fluid flow.
- The 3D printed microfluidic device was demonstrated to isolate CTCs from human blood samples.
- The capture efficacy using antibody-modified 3D printed microfluidic devices can reach as high as 90%.
- The isolation of CTCs from patient blood samples enables both early cancer diagnostics and treatment progresses.

23) Rostami, P., Kashaninejad, N., Moshksayan, K., Saidi, M. S., Firoozabadi, B., & Nguyen, N.-T. (2019). Novel approaches in cancer management with circulating tumor cell clusters. *Journal of Science: Advanced Materials and Devices*, 4(1), 1–18. doi: 10.1016/j.jsamd.2019.01.006

This paper focuses on new ways to separate circulating tumor cell clusters from a patient's bloodstream. While CTC cluster research is a fairly new field, the analysis of them can offer new insights into how tumors metastasize, which can lead to new ideas on how to cure cancer as a whole. This paper has a focus on passive separation methods, specifically designed for the separation of CTC clusters. The paper also thoroughly discusses the role of CTC clusters in metastasis, their physical and biological characteristics, clinical applications, and current challenges of CTC clusters.

Interestingly, this paper does not seem to have the main purpose of determining a patient's metastasis risk or separating CTC clusters to keep the patient from experiencing metastasis. Instead, the goal seems to be the separation of CTC clusters to study for research purposes. The paper discusses a number of different CTC cluster separation techniques in great detail, usually microfluidic, including antibody, physical property (cell density, size,

deformability), and photoacoustic. This paper is a great starting point to determine the type of cluster separation that could be best implemented into our design.

24) Zhang, J., Chen, K., & Fan, Z. H. (2016). Circulating Tumor Cell Isolation and Analysis. *Advanced Clinical Chemistry*, 1–31. doi: 10.1016/bs.acc.2016.03.003.

This review summarizes several methods of microfluidic CTC isolation and analysis, and their applications in clinical studies. At its basest level, cancers are analyzed primarily by biopsy, but this can be invasive and one-time tests. These microfluidic methods allow for fairly non-invasive tests to be performed on a regular basis. While microfluidics can allow for smaller blood samples, this also decreases the chance of a CTC to even be located in a blood sample, let alone to be found.

The most widely used method is immunomagnetic separation. This entails enriching CTCs based on the expression of surface proteins and capture agent-labeled magnetic beads using cell-surface markers of depleting white blood cells. There is also isolation based on physical properties, in which CTCs can be separated by such factors as size, density, deformability, or electric charges. The methods for such consist of centrifugation, membrane- or filtration-based systems, or dielectrophoresis (DEP). Another method is isolation by biological properties, such as surface antigens, cytoplasmic protein expression, and invasion capacity. This will entail typically adhering such biological systems to the CTCs and then detecting or removing those biological systems. The paper then goes on to discuss how to analyze CTCs, but that is not specifically relevant to this project, as we are mainly interested in the separation itself.

25) Adams André A., Okagbare, P. I., Feng, J., Hupert, M. L., Patterson, D., Göttert Jost, ... Soper, S. A. (2008). Highly Efficient Circulating Tumor Cell Isolation from Whole Blood and Label-Free Enumeration Using Polymer-Based Microfluidics with an Integrated Conductivity Sensor. *Journal of the American Chemical Society*, 130(27), 8633–8641. doi: 10.1021/ja8015022

This article illustrates a potential antibody-based isolation method for breast cancer CTCs. This allows larger volumes of blood (>1mL) to be filtered in a shorter time period (<37 minutes) than other microfluidic separators. This works by capturing the CTCs with antibodies, then once they are released, counting them with an integrated conductivity sensor. The device uses 51 high-aspect ratio microchannels covered in monoclonal antibodies to capture the EpCAM segment of the CTCs. This allows for whole blood filtering, with an efficiency of over 97%.

While this device might not work with clusters of CTCs, this could be applicable to the CD64 sepsis device, as that is also antibody based with minimal documentation. This device releases the captured CTCs using trypsin, as well as devising a way to count the CTCs as they pass, both of which could be used in our overall design.

26) Singer, K., Subbaiah, P., Hutchinson, R., Odetola, F., & Shanley, T. P. (2011). Clinical course of sepsis in children with acute leukemia admitted to the pediatric intensive care unit. *Pediatric Critical Care Medicine*, 12(6), 649–654. doi: 10.1097/pcc.0b013e31821927f1

While this article is mainly the abstract, we can still find relevance in a lot of the given data. The goal of this article was to describe the clinical course, resource use, and mortality of patients with leukemia admitted to the pediatric intensive care unit with sepsis and non-sepsis diagnoses over a 10-yr period (1998-2008). The main point of this article was that patients with acute leukemia and sepsis had a significantly higher mortality rate than standard pediatric sepsis mortality rates. While this seems to be a fairly obvious conclusion, it does show how linked these two diseases can be, and how deadly they can be. Treatments and their effectiveness was also briefly discussed but that is not relevant to our device.

48.5% of the leukemia admissions additionally had sepsis upon admission. Additionally, there was higher mortality among children with sepsis than other diagnoses (52% vs. 17%), and mortality among children with sepsis was higher among those with acute lymphoblastic leukemia (60% vs. 44%) compared to those with acute myelogenous leukemia.

27) DeAngelis, L. M. (2002). Leukemia and Lymphoma Metastases, 362–374. doi: 3601_e15_p362-374

This is one of the main articles on Leukemia metastasis. It describes statistics for CNS metastasis and was one of my main sources on Leptomeningeal Metastasis (LM). Both leukemia and lymphoma lead strongly into brain cancers, such as LM. LM can be particularly dangerous because it can mimic vincristine peripheral neuropathy, which is common among patients with lymphoma or leukemia. Patients with LM are also vulnerable to infections like sepsis, which can mimic LM symptoms.

The paper also discusses the clinical features, diagnosis, initial management, and treatment of epidural metastases (spinal cord) and LM (brain meninges). If a patient develops LM, their prognosis is very grim, with a median survival of 6-10 months, depending on the type of leukemia that created it. This is partially because LM is usually a late complication of leukemia, but also because LM is immune to chemotherapy due to the blood-brain barrier, and can cause spontaneous recurrence of cancer, typically in the brain.

28) Gauer, R. L. (2013). Early Recognition and Management of Sepsis in Adults: The First Six Hours. *American Family Physician*, 88(1), 44–53. Retrieved from <https://www.aafp.org/afp/2013/0701/p44.html>

This is one of the main articles for sepsis definition. Sepsis is a complication of severe infection characterized by a systemic inflammatory response. It is life-threatening, extremely common, aggressive, and displays a wide variety of symptoms, depending on the patient. Sepsis can manifest with anything from cold/clammy skin to abdominal pain, to headache, sore throat, chest pain, and many more. Basically any symptom of most common diseases, especially infectious diseases, could be an indicator of sepsis, because it is triggered by infection. This can make it very difficult to detect by physical symptoms alone.

The main symptoms of sepsis can be found within the body. Given that sepsis is a combination of systemic inflammatory response syndrome (SIRS) and an infection we need to

define what each of these are. While there are several different definition symptoms for SIRS, the main one for our device is WBC count, specifically a white blood cell count $> 12,000/\text{mm}^3$ or $< 4,000/\text{mm}^3$. Additionally, we can define severe sepsis as sepsis with a platelet count $< 100,000/\text{mL}$. Early management is also discussed, being implemented within 6 hours of suspected sepsis, and late management within the next six. We can see that the ideal window for sepsis diagnosis is within 6-7 hours of first occurrence, though sooner is preferred.

29) Malik, I. A., Cardenas-Turanzas, M., Gaeta, S., Borthakur, G., Price, K., Cortes, J., & Nates, J. L. (2017). Sepsis and Acute Myeloid Leukemia: A Population-Level Study of Comparative Outcomes of Patients Discharged From Texas Hospitals. *Clinical Lymphoma Myeloma and Leukemia*, 17(12). doi: 10.1016/j.clml.2017.07.009

This article displays statistics for adult leukemia patients, as well as how sepsis interacts with adult leukemia, specifically acute myeloid leukemia (AML). Of these studied patients, 40% were ≥ 65 years old, and 52% were men. Additionally, the rate of sepsis for AML patients was 16%, while it was only 4% for non-AML patients. Sepsis death was also 9% more common in AML patients than non-AML patients (30% compared to 21%). The combination of increase in sepsis incidence and mortality rates displays the need for rapid sepsis diagnosis in AML patients.

30) Bate, J., Gibson, F., Johnson, E., Selwood, K., Skinner, R., & Chisholm, J. (2013). Neutropenic sepsis: prevention and management of neutropenic sepsis in cancer patients (NICE Clinical Guideline CG151). *Archives of Disease in Childhood - Education & Practice Edition*, 98(2), 73–75. doi: 10.1136/archdischild-2013-303634

This article has to do with neutropenic sepsis, which is “an abnormal decrease in the number of neutrophils in the blood together with infection”. Neutropenic sepsis is also a complication of anticancer treatments, and can be life-threatening. The mortality risk and other risks of adverse clinical outcomes increase as the absolute neutrophil count (ANC) falls.

Treatment is typically decided by a combination of neutrophil count and fever. Specifically, an absolute neutrophil count of $< 0.5 \times 10^9$ /litre, or $< 1.0 \times 10^9$ /litre and falling.

This could have a huge impact on our project, given that we are planning to count a type of neutrophil to determine sepsis. Given that the overall number of neutrophils will decrease during neutropenic sepsis, it is safe to assume that the neutrophil type we are counting will also decrease.

Bibliography

Intro

- (1) Cancer. (n.d.). Retrieved from <https://www.who.int/news-room/fact-sheets/detail/cancer>
- (2) Number of Diagnoses: CureSearch. (2019, November 12). Retrieved from <https://curesearch.org/Number-of-Diagnoses>
- (3) Key Statistics for Childhood Cancers. (n.d.). Retrieved May 05, 2020, from <https://www.cancer.org/cancer/cancer-in-children/key-statistics.html>
- (4) 5-Year Survival Rate: CureSearch. (2019, November 13). Retrieved from <https://curesearch.org/5-Year-Survival-Rate>
- (5) Edd, J. F., Mishra, A., Dubash, T. D., Herrera, S., Mohammad, R., Williams, E. K., ... Toner, M. (2020). Microfluidic concentration and separation of circulating tumor cell clusters from large blood volumes. *Lab on a Chip*, 20(3), 558–567. doi: 10.1039/c9lc01122f
- (6) Deutsche Welle. (n.d.). Metastases – the real cancer risk: DW: 04.02.2019. Retrieved May 05, 2020, from <https://www.dw.com/en/metastases-the-real-cancer-risk/a-42709642>
- (7) Types of Childhood and Adolescent Cancers. (n.d.). Retrieved May 05, 2020, from <https://www.healthychildren.org/English/health-issues/conditions/cancer/Pages/Childhood-Cancer.aspx>
- (8) Children's Hospital. (2014, September 11). Pediatric Leukemias. Retrieved May 05, 2020, from <https://www.chop.edu/conditions-diseases/pediatric-leukemias>

- (9) How Fast Does Leukemia Develop? (n.d.). Retrieved May 05, 2020, from <https://www.roswellpark.org/cancertalk/201810/how-fast-does-leukemia-develop>
- (10) Hodgkin Lymphoma | Vanderbilt-Ingram Cancer Center. (n.d.). Retrieved May 5, 2020, from <https://www.vicc.org/cancer-info/adult-hodgkin-lymphoma>
- (11) DeAngelis, L. M. (2002). Leukemia and Lymphoma Metastases, 362–374. doi: 3601_e15_p362-374
- (12) Stages of cancer. (2019, July 23). Retrieved from <https://www.cancerresearchuk.org/about-cancer/what-is-cancer/stages-of-cancer>
- (13) Lymphoma - Non-Hodgkin - Childhood - Statistics. (2020, February 19). Retrieved from <https://www.cancer.net/cancer-types/lymphoma-non-hodgkin-childhood/statistics>
- (14) Five year survival rates by cancer type. (n.d.). Retrieved May 05, 2020, from <https://ourworldindata.org/grapher/five-year-survival-rates-by-cancer-type>
- (15) Gauer, R. L. (2013). Early Recognition and Management of Sepsis in Adults: The First Six Hours. *American Family Physician*, 88(1), 44–53. Retrieved from <https://www.aafp.org/afp/2013/0701/p44.html>
- (16) Hassan, U., Ghonge, T., Reddy, B., Patel, M., Rappleye, M., Taneja, I., . . . Bashir, R. (2017). A point-of-care microfluidic biochip for quantification of CD64 expression from whole blood for sepsis stratification. *Nature Communications*, 8(1). doi:10.1038/ncomms15949
- (17) Ingram, I. (2018, September 25). Sepsis in Pediatric ALL Tied to Long-Term Neuro Effects. Retrieved from <https://www.medpagetoday.com/hematologyoncology/leukemia/75286>
- (18) Fayed, L. (2020, January 27). Nadir Happens During Chemotherapy, But Why? Retrieved from <https://www.verywellhealth.com/nadir-and-chemotherapy-513861>

Project Overview

- (19) Au, S.H., Edd, J., Stoddard, A.E. et al. Microfluidic Isolation of Circulating Tumor Cell Clusters by Size and Asymmetry. *Sci Rep* 7, 2433 (2017).
<https://doi.org/10.1038/s41598-017-01150-3>
- (20) Lin et al. (2017). High-Throughput Microfluidic Labyrinth for the Label-free Isolation of Circulating Tumor Cells. *Cell Systems* 5, 295–304 September 27, 2017
<http://dx.doi.org/10.1016/j.cels.2017.08.012>

Background and Significance

- (21) Bankó, Petra et al. “Technologies for circulating tumor cell separation from whole blood.” *Journal of hematology & oncology* vol. 12,1 48. 14 May. 2019,
[doi:10.1186/s13045-019-0735-4](https://doi.org/10.1186/s13045-019-0735-4)
- (22) Jun Zhang, et al. “Fundamentals and Applications of Inertial Microfluidics: a Review.” *Lab on a Chip*, Royal Society of Chemistry, 3 Nov. 2015,
pubs.rsc.org/en/content/articlehtml/2015/lc/c5lc01159k
- (23) Lin, Eric et al. High-Throughput Microfluidic Labyrinth for the Label-free Isolation of Circulating Tumor Cells *Cell Systems*, Volume 5, Issue 3, 295 - 304.e4
<https://doi.org/10.1016/j.cels.2017.08.012>
- (24) Tae Hyun Kim, Hyeun Joong Yoon, Philip Stella, and Sunitha Nagrath. Cascaded spiral microfluidic device for deterministic and high purity continuous separation of circulating tumor cells. *Biomicrofluidics* 8, 064117 (2014). <https://doi.org/10.1063/1.4903501>
- (25) Wan, S., Kim, T.H., Smith, K.J. et al. New Labyrinth Microfluidic Device Detects Circulating Tumor Cells Expressing Cancer Stem Cell Marker and Circulating Tumor Microemboli in Hepatocellular Carcinoma. *Sci Rep* 9, 18575 (2019).
<https://doi.org/10.1038/s41598-019-54960-y>

- (26) Hassan, U., Ghonge, T., Reddy Jr., B. et al. A point-of-care microfluidic biochip for quantification of CD64 expression from whole blood for sepsis stratification. *Nat Commun* 8, 15949 (2017). <https://doi.org/10.1038/ncomms15949>

Subsystem Overview

- (27) Lin et al. (2017). High-Throughput Microfluidic Labyrinth for the Label-free Isolation of Circulating Tumor Cells. *Cell Systems* 5, 295–304 September 27, 2017
<http://dx.doi.org/10.1016/j.cels.2017.08.012>
- (28) Wan, S., Kim, T.H., Smith, K.J. et al. New Labyrinth Microfluidic Device Detects Circulating Tumor Cells Expressing Cancer Stem Cell Marker and Circulating Tumor Microemboli in Hepatocellular Carcinoma. *Sci Rep* 9, 18575 (2019).
<https://doi.org/10.1038/s41598-019-54960-y>
- (29) Au, S.H., Edd, J., Stoddard, A.E. et al. Microfluidic Isolation of Circulating Tumor Cell Clusters by Size and Asymmetry. *Sci Rep* 7, 2433 (2017).
<https://doi.org/10.1038/s41598-017-01150-3>
- (30) Wojtal, K. A., Rogler, G., Scharl, M., Biedermann, L., Frei, P., Fried, M., Weber, A., Eloranta, J. J., Kullak-Ublick, G. A., & Vavricka, S. R. (2012). Fc gamma receptor CD64 modulates the inhibitory activity of infliximab. *PloS one*, 7(8), e43361.
<https://doi.org/10.1371/journal.pone.0043361>
- (31) Chen, M., Ma, Z., Wu, X. et al. A molecular beacon-based approach for live-cell imaging of RNA transcripts with minimal target engineering at the single-molecule level. *Sci Rep* 7, 1550 (2017). <https://doi.org/10.1038/s41598-017-01740-1>

System Integration

- (32) Gauer, R. L. (2013). Early Recognition and Management of Sepsis in Adults: The First Six Hours. *American Family Physician*, 88(1), 44–53. Retrieved from
<https://www.aafp.org/afp/2013/0701/p44.html>

(33) Hodgkin Lymphoma: Vanderbilt-Ingram Cancer Center. (2019, November 26). Retrieved from <https://www.vicc.org/cancer-info/adult-hodgkin-lymphoma>

(34) Wang, E. (2018, October 4). How Fast Does Leukemia Develop? Retrieved from <https://www.roswellpark.org/cancertalk/201810/how-fast-does-leukemia-develop>

Results

(35) Horna P, Deaver DM, Qin D, et al. Quantitative flow cytometric identification of aberrant T cell clusters in erythrodermic cutaneous T cell lymphoma. Implications for staging and prognosis. *Journal of Clinical Pathology* 2014;67:431-436.

(36) Wan, S., Kim, T.H., Smith, K.J. et al. New Labyrinth Microfluidic Device Detects Circulating Tumor Cells Expressing Cancer Stem Cell Marker and Circulating Tumor Microemboli in Hepatocellular Carcinoma. *Sci Rep* 9, 18575 (2019). <https://doi.org/10.1038/s41598-019-54960-y>

(37) Wojtal, K. A., Rogler, G., Scharl, M., Biedermann, L., Frei, P., Fried, M., Weber, A., Eloranta, J. J., Kullak-Ublick, G. A., & Vavricka, S. R. (2012). Fc gamma receptor CD64 modulates the inhibitory activity of infliximab. *PloS one*, 7(8), e43361. <https://doi.org/10.1371/journal.pone.0043361>

Engineering Standards

(38) Marwaha, R. K., Kulkarni, K. P., Bansal, D., & Trehan, A. (2010). Pattern of Mortality in Childhood Acute Lymphoblastic Leukemia. *Journal of Pediatric Hematology/Oncology*, 32(5), 366-369. doi:10.1097/mpb.0b013e3181e0d036

Appendix

(A1) Hassan, U., Ghonge, T., Reddy Jr., B. *et al.* A point-of-care microfluidic biochip for quantification of CD64 expression from whole blood for sepsis stratification. *Nat Commun* 8, 15949 (2017). <https://doi.org/10.1038/ncomms15949>

(A2) Au, S.H., Edd, J., Stoddard, A.E. *et al.* Microfluidic Isolation of Circulating Tumor Cell Clusters by Size and Asymmetry. *Sci Rep* 7, 2433 (2017).
<https://doi.org/10.1038/s41598-017-01150-3>

Figures

(F1) Singh, M., Bakhshinyan, D., Venugopal, C., & Singh, S. K.. (2017). Preclinical Modeling and Therapeutic Avenues for Cancer Metastasis to the Central Nervous System. *Frontiers in Oncology*. *Frontiers in Oncology*. <http://doi.org/10.3389/fonc.2017.00220>

(F2) Lozar, T., Gersak, K., Cemazar, M., Kuhar, C. G., & Jesenko, T. (2019). The biology and clinical potential of circulating tumor cells. *Radiology and oncology*, 53(2), 131–147.
<https://doi.org/10.2478/raon-2019-0024>

(F3) Kim, T. H., Yoon, H. J., Stella, P., & Nagrath, S. (2014). Cascaded spiral microfluidic device for deterministic and high purity continuous separation of circulating tumor cells. *Biomicrofluidics*, 8(6), 064117. <https://doi.org/10.1063/1.4903501>

(F4) Lin et al. (2017). High-Throughput Microfluidic Labyrinth for the Label-free Isolation of Circulating Tumor Cells. *Cell Systems* 5, 295–304 September 27, 2017
<http://dx.doi.org/10.1016/j.cels.2017.08.012>

(F5) Crisalli, P., & Kool, E. T. (2011). Multi-path quenchers: efficient quenching of common fluorophores. *Bioconjugate chemistry*, 22(11), 2345–2354.
<https://doi.org/10.1021/bc200424r>

(F6) Au, S.H., Edd, J., Stoddard, A.E. *et al.* Microfluidic Isolation of Circulating Tumor Cell Clusters by Size and Asymmetry. *Sci Rep* 7, 2433 (2017).
<https://doi.org/10.1038/s41598-017-01150-3>

(F7) Ying, Y., Lin, Y. Inertial Focusing and Separation of Particles in Similar Curved Channels. *Sci Rep* 9, 16575 (2019). <https://doi.org/10.1038/s41598-019-52983-z>

(F8) Wan, S., Kim, T.H., Smith, K.J. et al. New Labyrinth Microfluidic Device Detects Circulating Tumor Cells Expressing Cancer Stem Cell Marker and Circulating Tumor Microemboli in Hepatocellular Carcinoma. *Sci Rep* 9, 18575 (2019).
<https://doi.org/10.1038/s41598-019-54960-y>

(F9) Weber, A., Eloranta, J. J., Kullak-Ublick, G. A., & Vavricka, S. R. (2012). Fc gamma receptor CD64 modulates the inhibitory activity of infliximab. *PloS one*, 7(8), e43361.
<https://doi.org/10.1371/journal.pone.0043361>